

Analysis of identified particle transverse momentum spectra produced in pp, p–Pb and Pb–Pb collisions at the LHC using Tsallis–Pareto-type distribution

Pei-Pin Yang^{1,*}, Mai-Ying Duan^{1,†}, Fu-Hu Liu^{1,‡}, Raghunath Sahoo^{2,3,§}

¹*Institute of Theoretical Physics & College of Physics and Electronic Engineering, State Key Laboratory of Quantum Optics and Quantum Optics Devices & Collaborative Innovation Center of Extreme Optics, Shanxi University, Taiyuan 030006, China*

²*Department of Physics, Indian Institute of Technology Indore, Indore 453552, India*

³*Experimental Physics Department, CERN, 1211 Geneva 23, Switzerland*

Abstract: In the framework of a multi-source thermal model at the quark level, we have analyzed transverse momentum spectra of hadrons measured by the ALICE Collaboration in proton–proton (pp or p – p) collisions at the center-of-mass energy of $\sqrt{s} = 7$ and 13 TeV, proton–lead (p –Pb) collisions at $\sqrt{s_{NN}} = 5.02$ TeV, and lead–lead (Pb–Pb) collisions at $\sqrt{s_{NN}} = 2.76$ TeV. For meson(baryon), the contributions of two(three) constituent quarks are considered, in which each quark contributes to hadron transverse momentum to obey the revised Tsallis–Pareto-type distribution (the TP-like function in short) with isotropic random azimuth. Three main parameters, namely, the revised index a_0 , effective temperature T , and entropy-related index n are obtained, which show the same tendency for small and large systems with respect to the centrality (or multiplicity) of events, rest mass of hadrons, and constituent mass of quarks.

Keywords: Transverse momentum spectra, Tsallis–Pareto distribution, constituent quarks, proton–proton and heavy-ion Collisions

PACS numbers: 12.40.Ee, 13.85.Hd, 24.10.Pa

I. INTRODUCTION

The deconfined high-temperature and high-density state of nuclear matter, called quark-gluon plasma (QGP) is often studied by ultra-relativistic nuclear collisions. The transverse momentum (p_T) spectra and ratios of identified hadrons provide a means to study the properties of matter created in these collisions and the mechanism by which quasi-free partons are transformed into observable hadrons. The relative contributions of different hadronization mechanisms rely on the change of hadron’s p_T . At low- p_T , recombination may be dominant, but at high- p_T , hadrons may originate from fragmentation processes. This mainly depends on the potential transverse

momentum distribution of quarks. Therefore, it is important to have the p_T -spectra of identified mesons and baryons in a wide p_T -range.

Unlike up (u) and down (d) quarks those form ordinary matter, strange (s) quarks do not exist in the form of valence quarks in the colliding species, but they are light enough to be produced in large quantities in the process of ultra-relativistic collisions. In the early state of high-energy collisions, strangeness is produced in hard (perturbative) $2 \rightarrow 2$ partonic scattering processes by flavor creation ($gg \rightarrow s\bar{s}$, $q\bar{q} \rightarrow s\bar{s}$) and flavor excitation ($gs \rightarrow gs$, $qs \rightarrow qs$). Strangeness is also created during the subsequent partonic evolution via gluon splitting process ($g \rightarrow s\bar{s}$). These processes tend to dominate the production of strange hadrons with high- p_T , and the production of strange hadrons with low- p_T is mainly dominated by non-perturbative processes.

The production of strange hadrons is suppressed compared to that of hadrons containing only u/d quarks, because s quarks need higher threshold energy to be ex-

*E-mails: peipinyangshanxi@163.com; yangpeipin@qq.com

†E-mail: duanmaiying@sxu.edu.cn

‡Correspondence: E-mails: fuhuliu@163.com; fuhuliu@sxu.edu.cn

§Correspondence: E-mails: Raghunath.Sahoo@cern.ch; raghnath@iiti.ac.in

cited. In basic particle-particle collisions, the degree of suppression of strange hadrons is an important parameter in the model analysis. Therefore, the measurement of strange hadron production imposes restrictions on the models. The study of strange and multi-strange particles in relativistic heavy-ion collisions is an important tool for exploring the properties of the strong interaction system. The particle spectra provide abundant information about the temperature and collective flow of the system, which reflects the dynamic freezing condition, where the inelastic collision stops. The enhancement of strangeness in heavy-ion collisions is one of the most important signals of QGP [1–3].

In the past decades, around the search for QGP, researchers have conducted extensive study on hadrons containing one or more s quarks [1, 4, 5]. However, the origin of the strangeness enhancement is not yet clear, when strangeness is also observed to be enhanced in proton-proton (pp or p - p) collisions [6, 7]. The azimuthal correlations and mass-dependent hardening of the p_T spectra observed in the high-multiplicity pp and proton-nucleus (pA or p - A) collisions are typically attributed to the formation of strongly interacting quark-gluon medium [8–19]. The abundance of strange particles at different center-of-mass energies is in accordance with the calculation of the thermal statistical model [20–22]. Strangeness, light flavor production, and heavy-ion collision dynamics provide evidences for the properties of fluid-like and collectiveness of the medium [23, 24]. Studying pp collisions under high multiplicity is of considerable significance, because it opens up the possibility of understanding nuclear reaction phenomena from a microscopic perspective.

Studies of high multiplicity charged particles in pp and proton-lead (p -Pb) collisions at the Large Hadron Collider (LHC) have shown striking similarities to lead-lead (Pb-Pb) collisions. The facts that the enhancements of (multi-)strange hadrons [11], azimuthal correlations and double-ridge structure [12, 13], nonzero elliptic flow (v_2) coefficients and other anisotropic flow measurements [25–30], mass ordering in hadron p_T spectra, and characteristic modifications of baryon to meson ratios [10], have shown that collective phenomena also exist in small collision systems. In addition, the continuous evolution of the ratio of light-flavor hadrons to pions in pp , p -Pb, and Pb-Pb collisions have been found as a function of charged particle multiplicity den-

sity [26, 31, 32]. The observed similarities indicate that there is a common underlying mechanism that determines the chemical composition that arises from these collisions. That is, typically interactions among partons exit in these collisions.

Recently, we considered contributor quarks and based on the Tsallis statistics [33–37], the available p_T spectra of various particles produced in collisions of small systems [pp , deuteron-gold (d -Au), p -Pb] and large systems [gold-gold (Au-Au) and Pb-Pb] at high energies were studied [38, 39], where we have used the convolution of two or three revised Tsallis-Pareto-type distribution (the TP-like function in short) [40–43]. The application of convolution means that we have considered the azimuths of contributor quarks to be the same or parallel to each other. A detailed consideration shows that the azimuths of contributor quarks may be isotropic and random which includes the parallel, vertical, and any other cases. The analytical expressions for parallel and vertical cases are available. For any other cases, we may use the Monte Carlo method, if it is difficult to give the analytical expression.

In the current work, in the framework of multi-source thermal model at the quark level, we use the Monte Carlo method to study the p_T spectra of identified hadrons produced in the collisions of different centralities (or multiplicities) with small systems (pp and p -Pb) and large system (Pb-Pb), including non-strange hadrons ($\pi^+ + \pi^-$ and $p + \bar{p}$), strange hadrons ($K^+ + K^-$, K_S^0 , $K^* + \bar{K}^*$, and $\Lambda + \bar{\Lambda}$), and multi-strange hadrons ($\Xi^- + \bar{\Xi}^+$ and $\Omega^- + \bar{\Omega}^+$). The azimuths of contributor or constituent quarks are isotropic and random. The size of transverse momentum of each quark contributed to hadron's p_T is assumed to obey the TP-like function. Mathematically, we study the synthesis of two or three vectors with changeable azimuths and sizes.

The p_T spectra in a wide range can reflect more dynamical information of the collision process. In order to verify the feasibility of the model and extract relevant parameters, we collected the experimental data of p_T spectra of identified hadrons produced in pp collisions at $\sqrt{s} = 7$ and 13 TeV [44–47], p -Pb collisions at $\sqrt{s_{NN}} = 5.02$ TeV [10, 48–50], and Pb-Pb collisions at $\sqrt{s_{NN}} = 2.76$ TeV [51–54], measured by the ALICE Collaboration.

The remainder of this paper is structured as follows. The formalism and method are described in Section II.

Results and discussion are given in Section III. In Section IV, we summarize our main observations with conclusions.

II. FORMALISM AND METHOD

Inspired by the SU(3) super polymorphism theory, in 1964, M. Gell-Mann proposed the quark model [55]. There are two commonly used masses of quarks. One is the current mass of quark, which refers to the mass in the Lagrangian of quantum field theory. The other is the constituent mass of quark that refers to the equivalent mass after the interaction with the gluon being included when considering the composition of hadrons. The quark model believes that a meson is composed of a quark and antiquark pair, and a baryon is composed of three quarks.

In our recent work [38, 39], the TP-like function used for the p_T spectra of hadrons is given by

$$f(p_T) = \frac{1}{N} \frac{dN}{dp_T} = C_0 p_T^{a_0} \left(1 + \frac{\sqrt{p_T^2 + m_0^2} - m_0}{nT} \right)^{-n}, \quad (1)$$

where N is the number of particles, C_0 is the normalization constant, a_0 is the revised factor, T is the effective temperature, n is the entropy-related index, and m_0 is the rest mass of given hadron. The three parameters a_0 , T , and n can be determined from the p_T spectra of hadrons.

According to the multi-source thermal model [56, 57], we think that the p_T spectra of hadrons are contributed by the contributor or constituent quarks. The transverse momentum of each quark contributed to p_T of given hadron is assumed to follow the TP-like function, too. We have the contribution, p_{ti} , of the i -th quark to be

$$f_i(p_{ti}) = \frac{1}{N_i} \frac{dN_i}{dp_{ti}} = C_i p_{ti}^{a_{0i}} \left(1 + \frac{\sqrt{p_{ti}^2 + m_{0i}^2} - m_{0i}}{nT} \right)^{-n}. \quad (2)$$

Here, N_i is number of the i -th quark, C_i is the normalization constant, and m_{0i} is the constituent mass of the i -th quark. A meson is composed of a quark and antiquark pair, so i is equal to 1 or 2, and a baryon is composed of 3 quarks, so i is equal to 1, 2 or 3. Regardless of the value of i , we always have $N_i = N$.

The relations between the transverse momentum vectors \mathbf{p}_{t1} and \mathbf{p}_{t2} of constituent quark and antiquark

pair for meson, and those among the transverse momentum vectors \mathbf{p}_{t1} , \mathbf{p}_{t2} , and \mathbf{p}_{t3} of constituent quarks for baryon, may be parallel, vertical, or of any azimuth ϕ_i . The analytical expressions for the parallel and vertical cases are available in Refs. [38, 39]. For the cases of any azimuths, we may use the Monte Carlo method [58, 59] to obtain p_T , if the analytical expression is not available.

To obtain a discrete value of p_{ti} that satisfies Eq. (2), we can perform the solution of

$$\int_0^{p_{ti}} f_i(p'_{ti}) dp'_{ti} < r_i < \int_0^{p_{ti} + \delta p_{ti}} f_i(p'_{ti}) dp'_{ti}. \quad (3)$$

Here, r_i is a random number uniformly distributed in $[0, 1]$, δp_{ti} denotes a small shift in p_{ti} . To obtain a discrete value of ϕ_i that satisfies the isotropic or uniform distribution, we have

$$\phi_i = 2\pi R_i, \quad (4)$$

where R_i denotes a random number uniformly distributed in $[0, 1]$.

For a meson composed of a quark and antiquark pair, we have,

$$p_T = \sqrt{\left(\sum_{i=1}^2 p_{ti} \cos \phi_i \right)^2 + \left(\sum_{i=1}^2 p_{ti} \sin \phi_i \right)^2} = \sqrt{p_{t1}^2 + p_{t2}^2 + 2p_{t1}p_{t2} \cos |\phi_1 - \phi_2|}. \quad (5)$$

For a baryon composed of three quarks, we have,

$$p_T = \sqrt{\left(\sum_{i=1}^3 p_{ti} \cos \phi_i \right)^2 + \left(\sum_{i=1}^3 p_{ti} \sin \phi_i \right)^2} = \left(p_{t1}^2 + p_{t2}^2 + p_{t3}^2 + 2p_{t1}p_{t2} \cos |\phi_1 - \phi_2| + 2p_{t1}p_{t3} \cos |\phi_1 - \phi_3| + 2p_{t2}p_{t3} \cos |\phi_2 - \phi_3| \right)^{1/2}. \quad (6)$$

As the expression of p_T for hadron with 2 or 3 quarks, Eq. (5) or (6) can be easily extended to the hadron with multiple quarks, e.g. the hadron with 4 or 5 quarks. We have the expression of p_T for hadron with k quarks to be

$$p_T = \sqrt{\left(\sum_{i=1}^k p_{ti} \cos \phi_i \right)^2 + \left(\sum_{i=1}^k p_{ti} \sin \phi_i \right)^2}. \quad (7)$$

In fact, Eq. (7) is a uniform expression for p_T of any hadron. In a real calculation, we need k sets of p_{ti} and ϕ_i for a given p_T . After the calculation for many times, the distribution of p_T can be obtained in statistics.

It is worth emphasized that in the analysis performed in this paper, the mass of the quark is the constituent mass, but not the current mass [60, 61]. Our attempts show that the constituent mass is more suitable for the fit. Meanwhile, we need to always distinguish the transverse momentum, p_T of a given hadron and the transverse momentum p_{ti} of the i -th constituent quark with the azimuth ϕ_i .

III. RESULTS AND DISCUSSION

A. Comparison with data

Figure 1 shows the multiplicity dependent p_T spectra, the double-differential yield $(1/N_{evt})d^2N/dp_T dy$, of $\pi^+ + \pi^-$ (a), $K^+ + K^-$ (b), $p + \bar{p}$ (c), K_S^0 (d), $K^* + \bar{K}^*$ (e), $\Lambda + \bar{\Lambda}$ (f), $\Xi^- + \bar{\Xi}^+$ (g), and $\Omega^- + \bar{\Omega}^+$ (h) with rapidity $|y| < 0.5$, produced in pp collisions at the center-of-mass energy, $\sqrt{s} = 7$ TeV, where N_{evt} denotes the number of events which can be omitted in the vertical axis according to the format in the cited reference. Different symbols represent the experimental data for different multiplicity classes determined by the values of multiplicity (VOM) measured by the ALICE Collaboration [44], where in most cases the data are scaled by constant multipliers marked in the panels for clarity. The curves represent our fit results from the Monte Carlo calculations. The values of free parameters (a_0 , T , and n), normalization constant (N_0), χ^2 , and number of degree of freedom (ndof) are listed in Table 1 in which the particle type, quark structure that makes up hadrons, and form of spectra are mentioned. The corresponding serial numbers of VOM classes marked with the Roman numerals in the figure are also listed in Table 1 in terms of the percentage classes which can be regarded as the centrality classes. One can see that our fit results are in well agreement with the experiment data measured by the ALICE Collaboration at midrapidity in pp collisions at $\sqrt{s} = 7$ TeV.

Similar to Figure 1, Figure 2 shows the multiplicity dependent p_T spectra, the double-differential yield $(1/N_{evt})d^2N/dp_T dy$, of $\pi^+ + \pi^-$ (a), $K^+ + K^-$ (b), $p + \bar{p}$ (c), K_S^0 (d), K^{*0} (e), $\Lambda + \bar{\Lambda}$ (f), $\Xi^- + \bar{\Xi}^+$ (g), and $\Omega^- + \bar{\Omega}^+$ (h) with $|y| < 0.5$, produced in pp collisions at $\sqrt{s} = 13$ TeV measured by the ALICE Collaboration [45–47]. Different symbols represent the data for different serial num-

bers of VOM classes marked by the Roman numerals, and the corresponding centrality classes are listed in Table 2. The curves are our results of the Monte Carlo calculations which are used to fit the data. Some of the data are scaled by multiplying different amounts marked in the panels for clarity. The values of a_0 , T , n , N , χ^2/ndof , and other related information are listed in Table 2. From the figure and χ^2/ndof , one can see that our fit results are in good agreement with the experimental data measured by the ALICE Collaboration at midrapidity in pp collisions at $\sqrt{s} = 13$ TeV.

Similar to Figures 1 and 2, Figure 3 displays the centrality dependent p_T spectra, the invariant yield $(1/2\pi p_T)d^2N/dp_T dy$ (a–c) or $(1/N_{evt}2\pi p_T)d^2N/dp_T dy$ (d, f–h) or the double-differential yield $(1/N_{evt})d^2N/dp_T dy$ (e), of $\pi^+ + \pi^-$ (a), $K^+ + K^-$ (b), $p + \bar{p}$ (c), K_S^0 (d), $\Sigma(1385)^+$ (e), $\Lambda + \bar{\Lambda}$ (f), $(\Xi^- + \bar{\Xi}^+)/2$ (g), and $(\Omega^- + \bar{\Omega}^+)/2$ (h) with $-0.5 < y < 0$ (a–c, e, g, h) or $0 < y < 0.5$ (d, f), produced in p -Pb collisions at $\sqrt{s_{NN}} = 5.02$ TeV measured by the ALICE Collaboration [10, 48–50]. Different symbols represent the experimental data with different centrality classes, where different constant multipliers are used to re-scale the data for clarity. The curves are our fit results based on the Monte Carlo calculations. The values of a_0 , T , n , N_0 , and χ^2/ndof are listed in Table 3 with other information. One can see that our fit results are in good agreement with the experimental data measured by the ALICE Collaboration at mid- y in p -Pb collisions at $\sqrt{s_{NN}} = 5.02$ TeV.

Similar to Figures 1–3, Figure 4 gives the centrality dependent p_T spectra, the invariant yield $(1/2\pi p_T)d^2N/dp_T dy$ (a–c, e) or the double-differential yield $(1/N_{evt})d^2N/dp_T dy$ (d, f–h), of $\pi^+ + \pi^-$ (a), $K^+ + K^-$ (b), $p + \bar{p}$ (c), K_S^0 (d), $(K^{*0} + \bar{K}^{*0})/2$ (e), Λ (f), $(\Xi^- + \bar{\Xi}^+)/2$ (g), and $(\Omega^- + \bar{\Omega}^+)/2$ (h) with $|\eta| < 0.8$ (a–c) or $|y| < 0.5$ (d–h), produced in Pb–Pb collisions at $\sqrt{s_{NN}} = 2.76$ TeV measured by the ALICE Collaboration [51–54]. The symbols represent the experimental data and the curves are our fit results. The value of a_0 , T , n , N_0 , and χ^2/ndof are listed in Table 4. One can see that our fit results are approximately in agreement with the experimental data measured by the ALICE Collaborations at mid- η or mid- y in Pb–Pb collisions at $\sqrt{s_{NN}} = 2.76$ TeV.

From the above comparisons one can see that the multi-source thermal model at the quark level can fit the

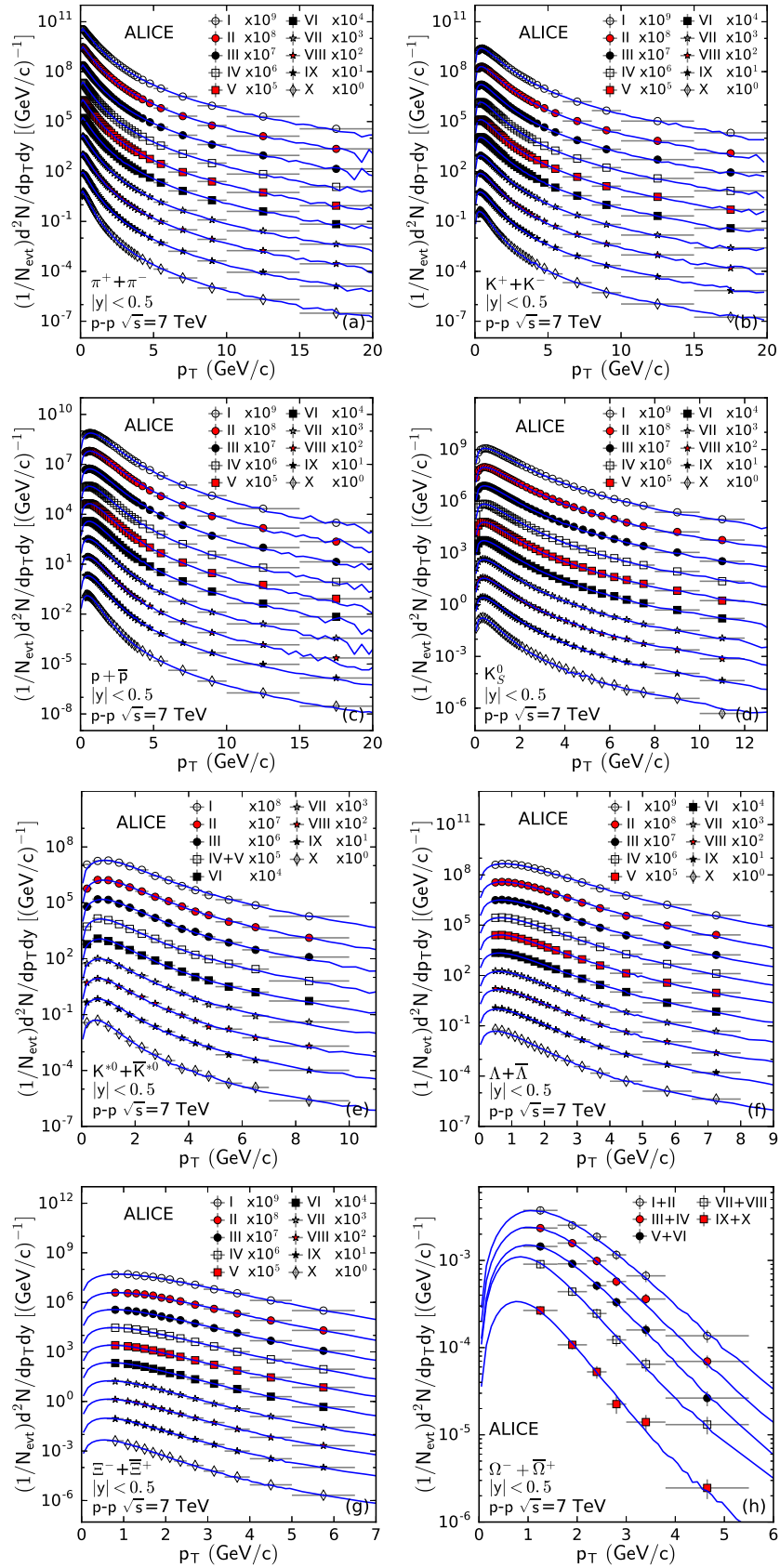


Fig. 1. Multiplicity dependent p_T spectra of $\pi^+ + \pi^-$ (a), $K^+ + K^-$ (b), $p + \bar{p}$ (c), K_S^0 (d), $K^* + \bar{K}^*$ (e), $\Lambda + \bar{\Lambda}$ (f), $\Xi^- + \bar{\Xi}^+$ (g), and $\Omega^- + \bar{\Omega}^+$ (h) with $|y| < 0.5$, produced in pp collisions at $\sqrt{s} = 7$ TeV. Different symbols represent the experimental data for different multiplicity classes measured by the ALICE Collaboration [44], where in most cases the data are scaled by constant multipliers marked in the panels for clarity. The curves represent our fit results based on the Monte Carlo calculations.

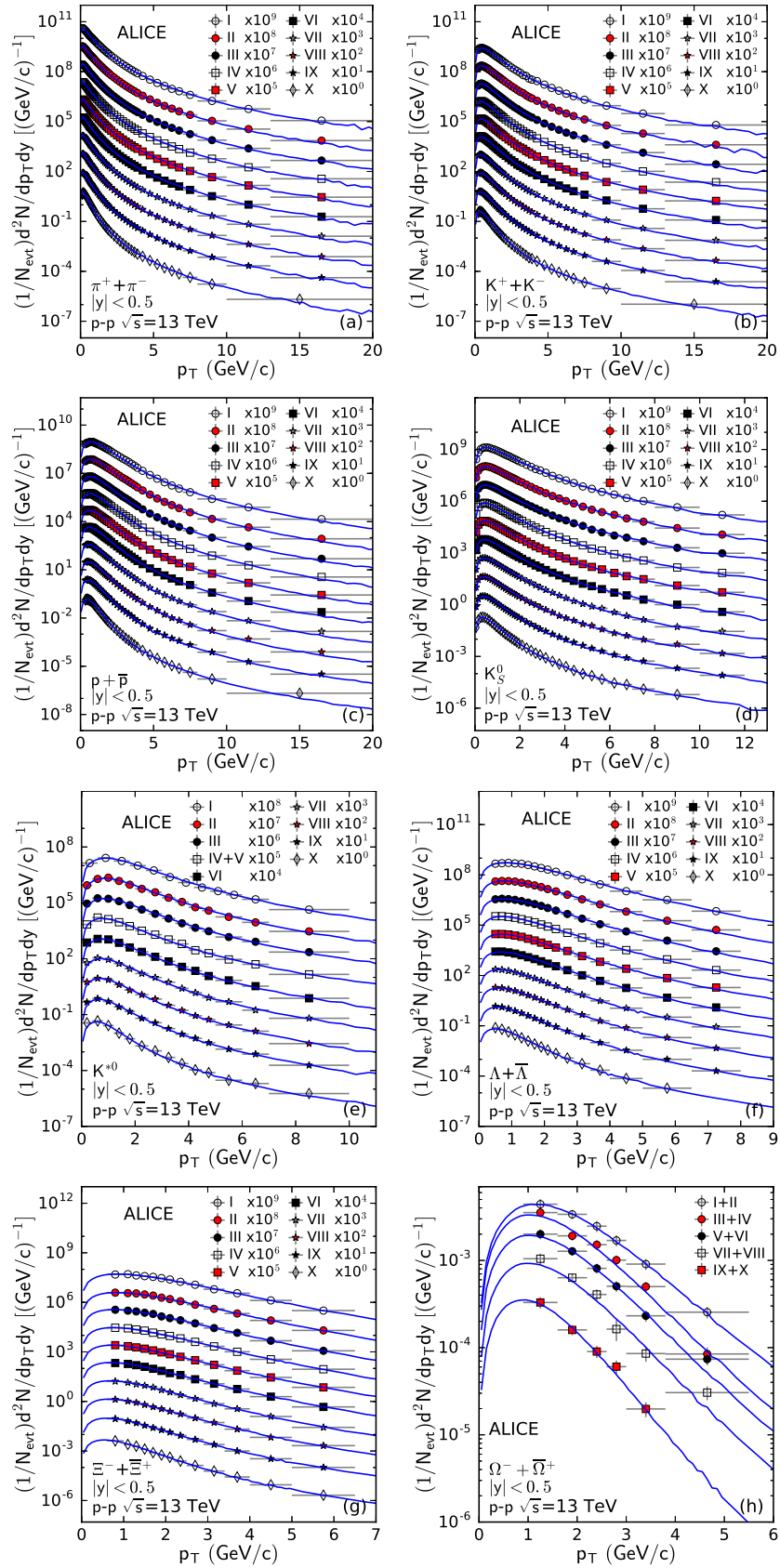


Fig. 2. Same as Figure 1, but showing the multiplicity dependent p_T spectra of $\pi^+ + \pi^-$ (a), $K^+ + K^-$ (b), $p + \bar{p}$ (c), K_S^0 (d), K^{*0} (e), $\Lambda + \bar{\Lambda}$ (f), $\Xi^- + \bar{\Xi}^+$ (g), and $\Omega^- + \bar{\Omega}^+$ (h) with $|y| < 0.5$ produced in pp collisions at $\sqrt{s} = 13$ TeV measured by the ALICE Collaboration [45–47].

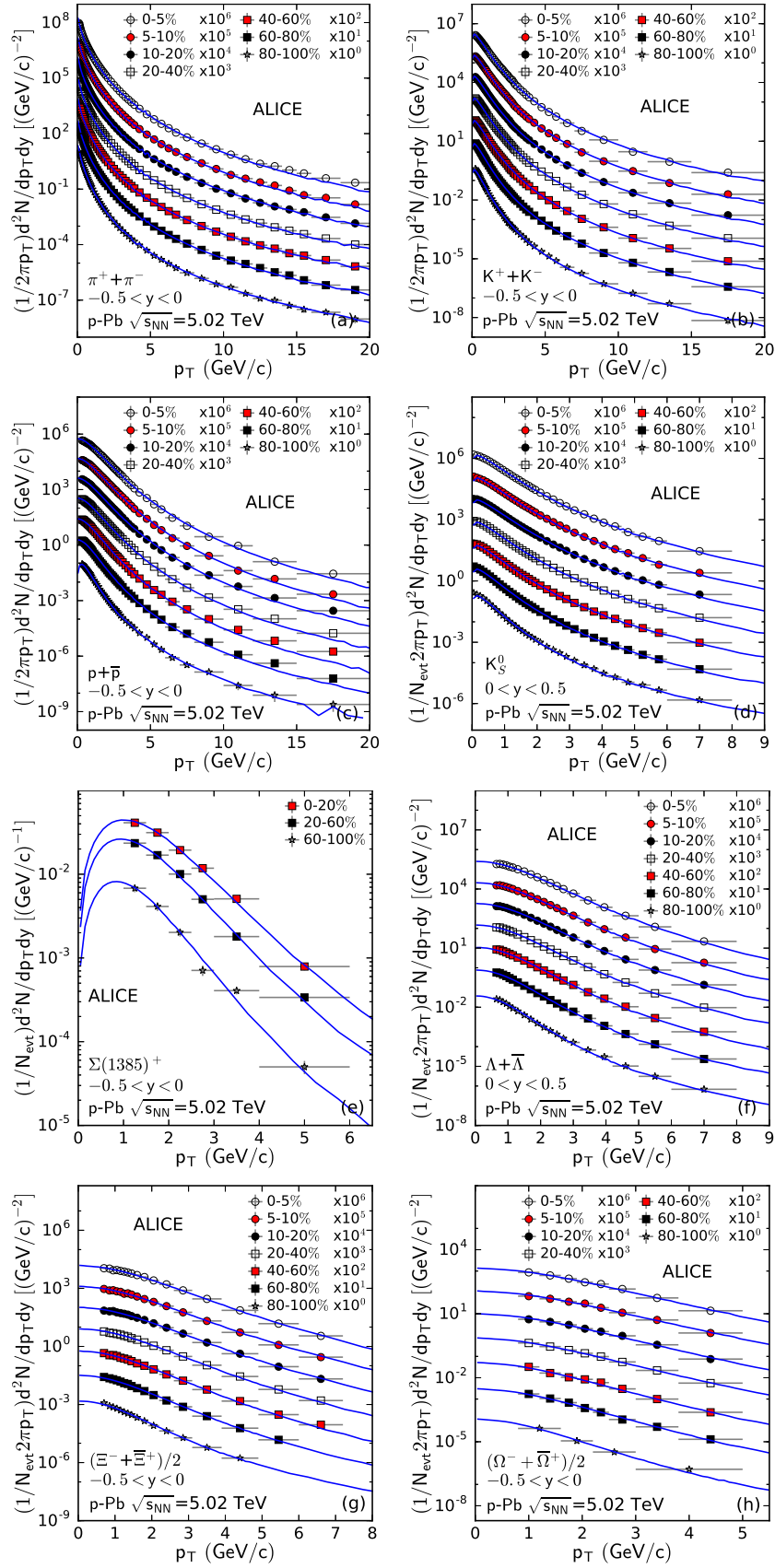


Fig. 3. The centrality dependent p_T spectra of $\pi^+ + \pi^-$ (a), $K^+ + K^-$ (b), $p + \bar{p}$ (c), K_S^0 (d), $\Sigma(1385)^+$ (e), $\Lambda + \bar{\Lambda}$ (f), $(\Xi^- + \Xi^+)/2$ (g), and $(\Omega^- + \Omega^+)/2$ (h) with $-0.5 < y < 0$ (a-c, e, g, h) or $0 < y < 0.5$ (d, f) produced in p -Pb collisions at $\sqrt{s_{NN}} = 5.02$ TeV measured by the ALICE Collaboration [10, 48–50]. Different symbols represent the experimental data with different centrality classes, where different constant multipliers are used to re-scale the data for clarity. The curves are our fit results based on the Monte Carlo calculations.

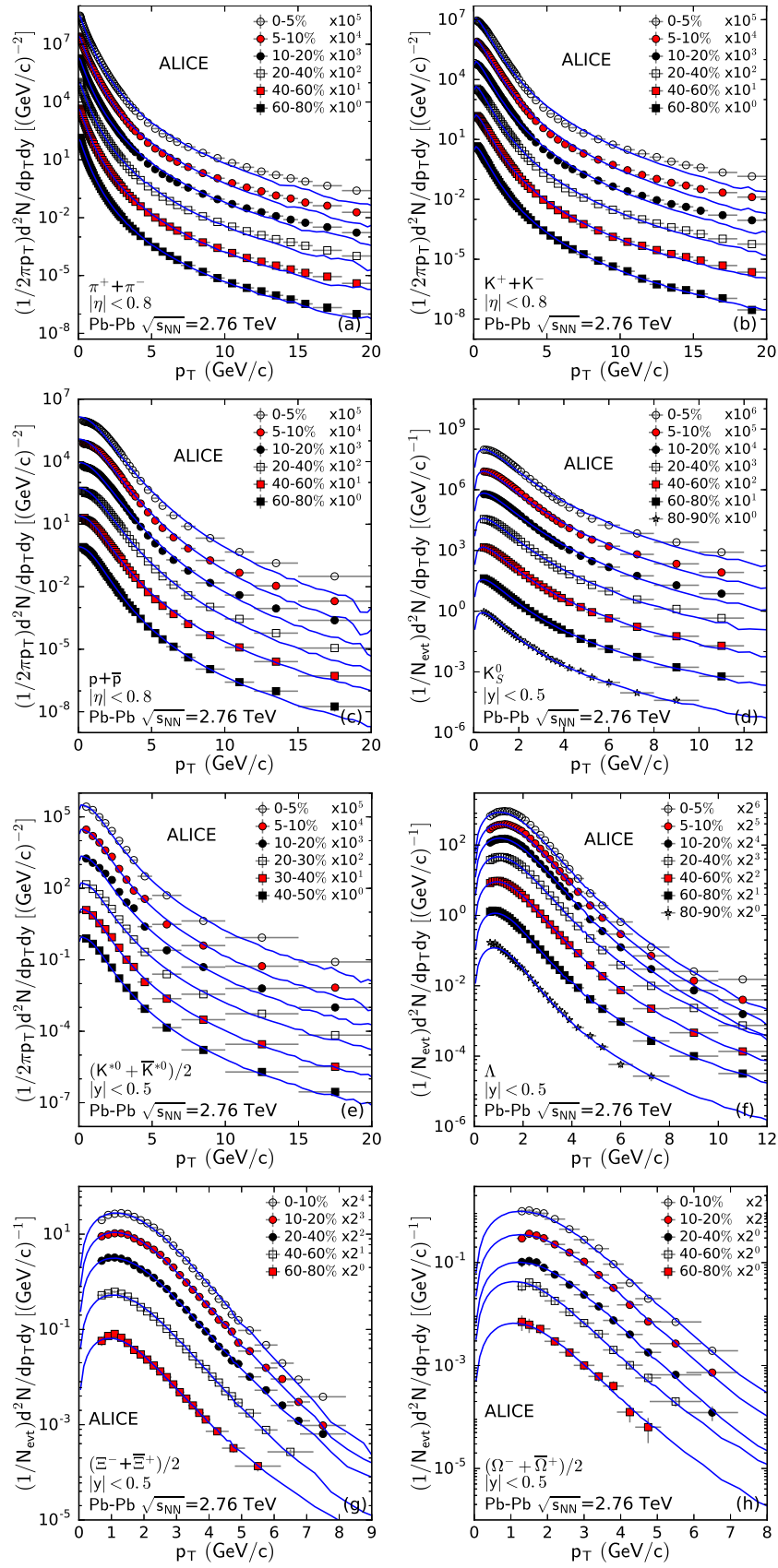


Fig. 4. Same as Figure 3, but showing the centrality dependent p_T spectra, of $\pi^+ + \pi^-$ (a), $K^+ + K^-$ (b), $p + \bar{p}$ (c), K_S^0 (d), $(K^{*0} + \bar{K}^{*0})/2$ (e), Λ (f), $(\Xi^- + \bar{\Xi}^+)/2$ (g), and $(\Omega^- + \bar{\Omega}^+)/2$ (h) with $|\eta| < 0.8$ (a-c) or $|y| < 0.5$ (d-h) produced in Pb-Pb collisions at $\sqrt{s_{NN}} = 2.76$ TeV measured by the ALICE Collaboration [51–54].

Table 1. Values of the free parameters (a_0 , T , and n), normalization constant (N_0), χ^2 , and ndof corresponding to the curves in Figure 1 for pp collisions at $\sqrt{s} = 7$ TeV. The particle type (quark structure), spectrum form, and multiplicity classes are given together. The multiplicity classes I, II, III, IV, V, VI, VII, VIII, IX, and X correspond to the centrality classes 0–0.95%, 0.95–4.7%, 4.7–9.5%, 9.5–14%, 14–19%, 19–28%, 28–38%, 38–48%, 48–68%, and 68–100%, respectively.

Particle (quark structure) and spectrum form	Multiplicity class	a_0	T (GeV)	n	N_0	χ^2/ndof
$\pi^+ + \pi^-$ ($u\bar{d}, d\bar{u}$) ($1/N_{evt}d^2N/dp_T dy$ [(GeV/c) $^{-1}$])	I	-0.550 ± 0.004	0.345 ± 0.002	5.071 ± 0.054	$(2.130 \pm 0.042) \times 10^1$	58/44
	II	-0.550 ± 0.003	0.321 ± 0.003	4.962 ± 0.035	$(1.700 \pm 0.021) \times 10^1$	66/44
	III	-0.550 ± 0.004	0.313 ± 0.002	4.962 ± 0.031	$(1.350 \pm 0.040) \times 10^1$	69/44
	IV	-0.550 ± 0.004	0.299 ± 0.002	4.934 ± 0.066	$(1.200 \pm 0.030) \times 10^1$	66/44
	V	-0.550 ± 0.005	0.291 ± 0.001	4.910 ± 0.033	$(1.040 \pm 0.101) \times 10^1$	65/44
	VI	-0.550 ± 0.005	0.287 ± 0.001	4.906 ± 0.029	$(8.580 \pm 0.080) \times 10^0$	84/44
	VII	-0.550 ± 0.004	0.266 ± 0.002	4.910 ± 0.086	$(7.230 \pm 0.040) \times 10^0$	62/44
	VIII	-0.550 ± 0.003	0.254 ± 0.002	4.910 ± 0.115	$(5.860 \pm 0.030) \times 10^0$	69/44
	IX	-0.550 ± 0.003	0.233 ± 0.001	4.916 ± 0.041	$(4.370 \pm 0.101) \times 10^0$	104/44
	X	-0.550 ± 0.005	0.187 ± 0.002	4.910 ± 0.032	$(2.750 \pm 0.080) \times 10^0$	194/44
$K^+ + K^-$ ($u\bar{s}, s\bar{u}$) ($1/N_{evt}d^2N/dp_T dy$ [(GeV/c) $^{-1}$])	I	0.148 ± 0.010	0.260 ± 0.002	5.325 ± 0.028	$(2.810 \pm 0.080) \times 10^0$	23/39
	II	0.148 ± 0.012	0.248 ± 0.001	5.321 ± 0.026	$(2.140 \pm 0.040) \times 10^0$	11/39
	III	0.148 ± 0.024	0.237 ± 0.002	5.260 ± 0.018	$(1.740 \pm 0.020) \times 10^0$	7/39
	IV	0.148 ± 0.016	0.230 ± 0.001	5.260 ± 0.014	$(1.490 \pm 0.020) \times 10^0$	6/39
	V	0.148 ± 0.016	0.224 ± 0.001	5.260 ± 0.014	$(1.300 \pm 0.010) \times 10^0$	5/39
	VI	0.148 ± 0.020	0.216 ± 0.001	5.261 ± 0.018	$(1.090 \pm 0.020) \times 10^0$	10/39
	VII	0.148 ± 0.016	0.207 ± 0.001	5.252 ± 0.023	$(8.500 \pm 0.080) \times 10^{-1}$	11/39
	VIII	0.148 ± 0.018	0.194 ± 0.001	5.240 ± 0.025	$(6.860 \pm 0.100) \times 10^{-1}$	17/39
	IX	0.148 ± 0.016	0.178 ± 0.001	5.214 ± 0.029	$(5.000 \pm 0.060) \times 10^{-1}$	22/39
	X	0.148 ± 0.021	0.146 ± 0.002	5.220 ± 0.030	$(2.900 \pm 0.060) \times 10^{-1}$	34/39
$p + \bar{p}$ ($uud, \bar{u}\bar{u}\bar{d}$) ($1/N_{evt}d^2N/dp_T dy$ [(GeV/c) $^{-1}$])	I	0.530 ± 0.008	0.214 ± 0.002	6.645 ± 0.035	$(1.109 \pm 0.009) \times 10^0$	5/37
	II	0.530 ± 0.005	0.205 ± 0.002	6.646 ± 0.075	$(8.701 \pm 0.150) \times 10^{-1}$	20/37
	III	0.530 ± 0.008	0.194 ± 0.001	6.579 ± 0.063	$(7.079 \pm 0.040) \times 10^{-1}$	17/37
	IV	0.530 ± 0.009	0.185 ± 0.001	6.603 ± 0.046	$(6.130 \pm 0.080) \times 10^{-1}$	14/37
	V	0.530 ± 0.008	0.178 ± 0.003	6.580 ± 0.086	$(5.450 \pm 0.090) \times 10^{-1}$	23/37
	VI	0.530 ± 0.011	0.170 ± 0.001	6.480 ± 0.080	$(4.530 \pm 0.080) \times 10^{-1}$	24/37
	VII	0.530 ± 0.004	0.157 ± 0.002	6.353 ± 0.066	$(3.650 \pm 0.060) \times 10^{-1}$	16/37
	VIII	0.530 ± 0.009	0.147 ± 0.001	6.341 ± 0.077	$(2.900 \pm 0.050) \times 10^{-1}$	22/37
	IX	0.530 ± 0.008	0.134 ± 0.001	6.181 ± 0.076	$(2.079 \pm 0.020) \times 10^{-1}$	25/37
	X	0.530 ± 0.010	0.110 ± 0.001	6.180 ± 0.065	$(1.120 \pm 0.020) \times 10^{-1}$	21/37
K_S^0 ($d\bar{s}$) ($1/N_{evt}d^2N/dp_T dy$ [(GeV/c) $^{-1}$])	I	0.148 ± 0.008	0.281 ± 0.002	5.722 ± 0.046	$(1.338 \pm 0.015) \times 10^0$	10/34
	II	0.148 ± 0.007	0.269 ± 0.002	5.720 ± 0.057	$(1.030 \pm 0.010) \times 10^0$	35/34
	III	0.148 ± 0.008	0.257 ± 0.001	5.716 ± 0.045	$(8.360 \pm 0.010) \times 10^{-1}$	29/34
	IV	0.148 ± 0.009	0.247 ± 0.002	5.625 ± 0.057	$(7.080 \pm 0.080) \times 10^{-1}$	35/34
	V	0.148 ± 0.008	0.239 ± 0.002	5.560 ± 0.057	$(6.200 \pm 0.080) \times 10^{-1}$	34/34
	VI	0.148 ± 0.011	0.231 ± 0.001	5.545 ± 0.066	$(5.150 \pm 0.060) \times 10^{-1}$	46/34
	VII	0.148 ± 0.008	0.222 ± 0.001	5.538 ± 0.088	$(4.000 \pm 0.040) \times 10^{-1}$	70/34
	VIII	0.148 ± 0.010	0.210 ± 0.001	5.480 ± 0.118	$(3.220 \pm 0.040) \times 10^{-1}$	70/34
	IX	0.148 ± 0.007	0.194 ± 0.001	5.444 ± 0.096	$(2.350 \pm 0.030) \times 10^{-1}$	63/34
	X	0.148 ± 0.011	0.154 ± 0.001	5.200 ± 0.057	$(1.270 \pm 0.020) \times 10^{-1}$	35/34

Table 1. Continued.

Particle (quark structure) and spectrum form	Multiplicity class	a_0	T (GeV)	n	N_0	χ^2/ndof
$K^{*0} + \bar{K}^{*0}$ ($u\bar{s}, s\bar{u}$) $(1/N_{evt})d^2N/dp_T dy$ [(GeV/c) $^{-1}$]	I	1.450 ± 0.012	0.196 ± 0.001	7.073 ± 0.030	$(3.250 \pm 0.040) \times 10^{-1}$	5/10
	II	1.450 ± 0.006	0.186 ± 0.001	7.062 ± 0.039	$(2.700 \pm 0.029) \times 10^{-1}$	3/10
	III	1.450 ± 0.013	0.168 ± 0.002	6.780 ± 0.035	$(2.300 \pm 0.040) \times 10^{-1}$	5/10
	IV+V	1.450 ± 0.018	0.154 ± 0.002	6.569 ± 0.035	$(1.910 \pm 0.030) \times 10^{-1}$	3/10
	VI	1.450 ± 0.020	0.141 ± 0.002	6.376 ± 0.086	$(4.519 \pm 0.020) \times 10^{-1}$	9/10
	VII	1.450 ± 0.012	0.133 ± 0.002	6.365 ± 0.057	$(1.249 \pm 0.040) \times 10^{-1}$	9/10
	VIII	1.450 ± 0.016	0.124 ± 0.003	6.367 ± 0.066	$(1.039 \pm 0.020) \times 10^{-1}$	6/10
	IX	1.450 ± 0.014	0.114 ± 0.002	6.346 ± 0.108	$(7.800 \pm 0.040) \times 10^{-2}$	10/10
	X	1.450 ± 0.020	0.093 ± 0.002	6.315 ± 0.111	$(4.800 \pm 0.030) \times 10^{-2}$	10/10
	$\Lambda + \bar{\Lambda}$ ($uds, \bar{u}\bar{d}\bar{s}$) $(1/N_{evt})d^2N/dp_T dy$ [(GeV/c) $^{-1}$]	I	1.100 ± 0.004	0.177 ± 0.001	7.149 ± 0.021	$(7.619 \pm 0.089) \times 10^{-1}$
II		1.100 ± 0.004	0.166 ± 0.001	7.138 ± 0.036	$(5.900 \pm 0.070) \times 10^{-1}$	7/12
III		1.100 ± 0.006	0.158 ± 0.002	7.078 ± 0.038	$(4.700 \pm 0.060) \times 10^{-1}$	12/12
IV		1.100 ± 0.015	0.151 ± 0.002	6.996 ± 0.040	$(3.979 \pm 0.060) \times 10^{-1}$	16/12
V		1.100 ± 0.013	0.144 ± 0.002	6.868 ± 0.042	$(3.450 \pm 0.060) \times 10^{-1}$	16/12
VI		1.100 ± 0.022	0.136 ± 0.002	6.780 ± 0.061	$(2.850 \pm 0.040) \times 10^{-1}$	18/12
VII		1.100 ± 0.014	0.126 ± 0.002	6.526 ± 0.075	$(2.200 \pm 0.039) \times 10^{-1}$	21/12
VIII		1.100 ± 0.011	0.118 ± 0.003	6.470 ± 0.103	$(1.720 \pm 0.040) \times 10^{-1}$	27/12
IX		1.100 ± 0.012	0.111 ± 0.002	6.476 ± 0.085	$(1.130 \pm 0.030) \times 10^{-1}$	23/12
X		1.100 ± 0.023	0.100 ± 0.002	6.476 ± 0.129	$(4.500 \pm 0.010) \times 10^{-2}$	29/12
$\Xi^- + \bar{\Xi}^+$ ($ssd, \bar{s}\bar{s}\bar{d}$) $(1/N_{evt})d^2N/dp_T dy$ [(GeV/c) $^{-1}$]	I	0.255 ± 0.004	0.396 ± 0.003	10.007 ± 0.060	$(9.700 \pm 0.069) \times 10^{-2}$	7/9
	II	0.255 ± 0.003	0.372 ± 0.001	9.615 ± 0.043	$(7.000 \pm 0.060) \times 10^{-2}$	10/9
	III	0.255 ± 0.006	0.328 ± 0.001	8.700 ± 0.026	$(6.000 \pm 0.060) \times 10^{-2}$	4/9
	IV	0.255 ± 0.005	0.320 ± 0.001	8.553 ± 0.034	$(4.800 \pm 0.019) \times 10^{-2}$	2/9
	V	0.255 ± 0.005	0.296 ± 0.001	7.629 ± 0.027	$(3.999 \pm 0.010) \times 10^{-2}$	4/9
	VI	0.255 ± 0.010	0.276 ± 0.001	7.366 ± 0.035	$(3.400 \pm 0.020) \times 10^{-2}$	3/9
	VII	0.255 ± 0.005	0.261 ± 0.001	7.306 ± 0.031	$(2.579 \pm 0.025) \times 10^{-2}$	4/9
	VIII	0.255 ± 0.007	0.242 ± 0.001	6.844 ± 0.035	$(1.899 \pm 0.010) \times 10^{-2}$	4/9
	IX	0.255 ± 0.006	0.210 ± 0.001	6.255 ± 0.018	$(1.240 \pm 0.012) \times 10^{-2}$	2/9
	X	0.255 ± 0.009	0.175 ± 0.001	6.060 ± 0.033	$(5.399 \pm 0.199) \times 10^{-3}$	4/9
$\Omega^- + \bar{\Omega}^+$ ($sss, \bar{s}\bar{s}\bar{s}$) $(1/N_{evt})d^2N/dp_T dy$ [(GeV/c) $^{-1}$]	I+II	0.830 ± 0.004	0.312 ± 0.002	9.597 ± 0.031	$(8.099 \pm 0.010) \times 10^{-3}$	1/2
	III+IV	0.830 ± 0.004	0.288 ± 0.002	9.548 ± 0.033	$(4.899 \pm 0.010) \times 10^{-3}$	2/2
	V+VI	0.830 ± 0.005	0.270 ± 0.002	9.572 ± 0.032	$(2.899 \pm 0.010) \times 10^{-3}$	1/2
	VII+VIII	0.830 ± 0.004	0.190 ± 0.002	6.477 ± 0.030	$(1.820 \pm 0.009) \times 10^{-3}$	1/2
	IX+X	0.830 ± 0.004	0.169 ± 0.002	6.477 ± 0.031	$(5.200 \pm 0.001) \times 10^{-4}$	3/2

p_T spectra of identified hadrons produced at midrapidity in pp , p -Pb, and Pb-Pb collisions at the LHC. We note that the degree of fit for pp collisions is better than that for p -Pb collisions, and the degree of fit for p -Pb collisions is better than that for Pb-Pb collisions. The phenomenon that the degree of fit for small system is better than that for large system is caused by the multiple scattering in large system. Due to the multiple scatter-

ing, there are more factors affecting particle production. In particular, in central Pb-Pb collisions, for light particles (π , K , and p) with high- p_T , the departure of the fit from data is more obvious. This is indeed caused by multiple scattering and other medium effects.

In the model, the contribution of each quark to p_T of given hadron is assumed to obey the TP-like function with isotropic azimuth. Although the analytical expres-

Table 2. Values of a_0 , T , n , N_0 , χ^2 , and ndof corresponding to the curves in Figure 2 for pp collisions at $\sqrt{s} = 13$ TeV. The particle type (quark structure), spectrum form, and multiplicity classes are given together. The multiplicity classes I, II, III, IV, V, VI, VII, VIII, IX, and X for $\pi^+ + \pi^-$, $K^+ + K^-$, and $p + \bar{p}$ correspond to the centrality classes 0–0.92%, 0.92–4.6%, 4.6–9.2%, 9.2–13.8%, 13.8–18.4%, 18.4–27.6%, 27.6–36.8%, 36.8–46%, 46–64.5%, and 64.5–100%, respectively, and for K_S^0 , K^{*0} , $\Lambda + \bar{\Lambda}$, $\Xi^- + \bar{\Xi}^+$, and $\Omega^- + \bar{\Omega}^+$ correspond to the centrality classes 0–0.9%, 0.9–4.5%, 4.5–8.9%, 8.9–13.5%, 13.5–18%, 18–27%, 27–36.1%, 36.1–45.3%, 45.3–64.5%, and 64.5–100%, respectively.

Particle (quark structure) and spectrum form	Multiplicity class	a_0	T (GeV)	n	N_0	χ^2/ndof
$\pi^+ + \pi^-$ ($u\bar{d}, d\bar{u}$) ($1/N_{evt}d^2N/dp_T dy$ [(GeV/c) $^{-1}$])	I	-0.550 ± 0.003	0.375 ± 0.002	4.996 ± 0.045	$(2.599 \pm 0.070) \times 10^1$	56/47
	II	-0.550 ± 0.002	0.350 ± 0.002	4.945 ± 0.022	$(2.030 \pm 0.030) \times 10^1$	74/47
	III	-0.550 ± 0.004	0.332 ± 0.004	4.870 ± 0.021	$(1.670 \pm 0.020) \times 10^1$	70/47
	IV	-0.550 ± 0.005	0.326 ± 0.002	4.874 ± 0.026	$(1.400 \pm 0.019) \times 10^1$	60/47
	V	-0.550 ± 0.005	0.315 ± 0.002	4.874 ± 0.035	$(1.250 \pm 0.002) \times 10^1$	55/47
	VI	-0.550 ± 0.005	0.305 ± 0.001	7.366 ± 0.020	$(1.030 \pm 0.014) \times 10^1$	44/47
	VII	-0.550 ± 0.002	0.288 ± 0.001	4.870 ± 0.016	$(8.229 \pm 0.089) \times 10^0$	49/47
	VIII	-0.550 ± 0.004	0.272 ± 0.001	4.870 ± 0.029	$(6.730 \pm 0.070) \times 10^0$	56/47
	IX	-0.550 ± 0.004	0.249 ± 0.001	4.865 ± 0.028	$(4.840 \pm 0.050) \times 10^0$	92/47
	X	-0.550 ± 0.005	0.203 ± 0.002	4.861 ± 0.022	$(2.800 \pm 0.050) \times 10^0$	324/47
$K^+ + K^-$ ($u\bar{s}, s\bar{u}$) ($1/N_{evt}d^2N/dp_T dy$ [(GeV/c) $^{-1}$])	I	0.148 ± 0.003	0.287 ± 0.003	5.276 ± 0.082	$(3.179 \pm 0.040) \times 10^0$	15/42
	II	0.148 ± 0.002	0.270 ± 0.002	5.273 ± 0.021	$(2.580 \pm 0.040) \times 10^0$	9/42
	III	0.148 ± 0.003	0.262 ± 0.001	5.273 ± 0.018	$(2.060 \pm 0.030) \times 10^0$	14/42
	IV	0.148 ± 0.005	0.254 ± 0.002	5.250 ± 0.021	$(1.740 \pm 0.019) \times 10^0$	25/42
	V	0.148 ± 0.005	0.243 ± 0.001	5.180 ± 0.022	$(1.540 \pm 0.020) \times 10^0$	24/42
	VI	0.148 ± 0.005	0.237 ± 0.003	5.242 ± 0.022	$(1.250 \pm 0.019) \times 10^0$	43/42
	VII	0.148 ± 0.004	0.224 ± 0.001	5.217 ± 0.023	$(9.799 \pm 0.100) \times 10^{-1}$	47/42
	VIII	0.148 ± 0.003	0.213 ± 0.002	5.223 ± 0.025	$(7.700 \pm 0.080) \times 10^{-1}$	54/42
	IX	0.148 ± 0.003	0.196 ± 0.002	5.199 ± 0.027	$(5.370 \pm 0.070) \times 10^{-1}$	67/42
	X	0.148 ± 0.005	0.158 ± 0.002	5.138 ± 0.024	$(2.970 \pm 0.040) \times 10^{-1}$	464/41
$p + \bar{p}$ ($uud, \bar{u}\bar{u}\bar{d}$) ($1/N_{evt}d^2N/dp_T dy$ [(GeV/c) $^{-1}$])	I	0.530 ± 0.011	0.224 ± 0.002	6.291 ± 0.012	$(1.379 \pm 0.029) \times 10^0$	24/40
	II	0.530 ± 0.013	0.208 ± 0.002	6.278 ± 0.096	$(1.060 \pm 0.020) \times 10^0$	24/40
	III	0.530 ± 0.012	0.197 ± 0.002	6.267 ± 0.044	$(8.799 \pm 0.149) \times 10^{-1}$	22/40
	IV	0.530 ± 0.011	0.193 ± 0.001	6.278 ± 0.012	$(7.299 \pm 0.090) \times 10^{-1}$	26/40
	V	0.530 ± 0.013	0.184 ± 0.003	6.262 ± 0.033	$(6.499 \pm 0.079) \times 10^{-1}$	20/40
	VI	0.530 ± 0.023	0.175 ± 0.001	6.247 ± 0.055	$(5.600 \pm 0.080) \times 10^{-1}$	27/40
	VII	0.530 ± 0.022	0.165 ± 0.002	6.240 ± 0.031	$(4.300 \pm 0.050) \times 10^{-1}$	31/40
	VIII	0.530 ± 0.015	0.155 ± 0.002	6.228 ± 0.033	$(3.450 \pm 0.060) \times 10^{-1}$	40/40
	IX	0.530 ± 0.009	0.141 ± 0.001	6.156 ± 0.036	$(2.360 \pm 0.040) \times 10^{-1}$	48/40
	X	0.530 ± 0.005	0.109 ± 0.001	5.914 ± 0.028	$(1.249 \pm 0.029) \times 10^{-1}$	36/40
K_S^0 ($d\bar{s}$) ($1/N_{evt}d^2N/dp_T dy$ [(GeV/c) $^{-1}$])	I	0.148 ± 0.003	0.304 ± 0.002	5.607 ± 0.033	$(1.610 \pm 0.019) \times 10^0$	18/34
	II	0.148 ± 0.005	0.288 ± 0.002	5.515 ± 0.038	$(1.210 \pm 0.080) \times 10^0$	33/34
	III	0.148 ± 0.004	0.273 ± 0.002	5.461 ± 0.063	$(9.899 \pm 0.079) \times 10^{-1}$	37/34
	IV	0.148 ± 0.003	0.257 ± 0.001	5.332 ± 0.032	$(8.500 \pm 0.040) \times 10^{-1}$	27/34
	V	0.148 ± 0.005	0.251 ± 0.002	5.302 ± 0.024	$(7.500 \pm 0.080) \times 10^{-1}$	35/34
	VI	0.148 ± 0.003	0.243 ± 0.001	5.303 ± 0.036	$(6.239 \pm 0.069) \times 10^{-1}$	54/34
	VII	0.148 ± 0.004	0.234 ± 0.002	5.337 ± 0.048	$(4.850 \pm 0.040) \times 10^{-1}$	65/34
	VIII	0.148 ± 0.004	0.218 ± 0.001	5.285 ± 0.043	$(3.930 \pm 0.050) \times 10^{-1}$	64/34
	IX	0.148 ± 0.003	0.200 ± 0.001	5.229 ± 0.008	$(2.760 \pm 0.030) \times 10^{-1}$	60/34
	X	0.148 ± 0.003	0.158 ± 0.001	5.000 ± 0.037	$(1.440 \pm 0.029) \times 10^{-1}$	51/34

Table 2. Continued.

Particle (quark structure) and spectrum form	Multiplicity class	a_0	T (GeV)	n	N_0	χ^2/ndof
K^{*0} ($d\bar{s}$) $(1/N_{evt})d^2N/dp_T dy$ [(GeV/c) $^{-1}$]	I	1.450 ± 0.022	0.209 ± 0.002	6.978 ± 0.013	$(4.569 \pm 0.150) \times 10^{-1}$	2/8
	II	1.450 ± 0.028	0.196 ± 0.002	6.925 ± 0.008	$(3.619 \pm 0.080) \times 10^{-1}$	8/10
	III	1.450 ± 0.035	0.190 ± 0.003	6.805 ± 0.013	$(2.899 \pm 0.070) \times 10^{-1}$	8/10
	IV+V	1.450 ± 0.030	0.166 ± 0.002	6.318 ± 0.016	$(2.379 \pm 0.010) \times 10^{-1}$	16/10
	VI	1.450 ± 0.028	0.166 ± 0.004	6.587 ± 0.006	$(1.829 \pm 0.089) \times 10^{-1}$	12/10
	VII	1.450 ± 0.018	0.153 ± 0.005	6.410 ± 0.008	$(1.519 \pm 0.040) \times 10^{-1}$	18/10
	VIII	1.450 ± 0.025	0.140 ± 0.003	6.415 ± 0.013	$(1.219 \pm 0.050) \times 10^{-1}$	17/10
	IX	1.450 ± 0.026	0.127 ± 0.002	6.224 ± 0.008	$(8.600 \pm 0.026) \times 10^{-2}$	17/10
	X	1.450 ± 0.018	0.103 ± 0.003	6.218 ± 0.007	$(4.700 \pm 0.029) \times 10^{-2}$	24/10
	$\Lambda + \bar{\Lambda}$ ($uds, \bar{u}\bar{d}\bar{s}$) $(1/N_{evt})d^2N/dp_T dy$ [(GeV/c) $^{-1}$]	I	0.300 ± 0.021	0.357 ± 0.003	8.885 ± 0.013	$(9.499 \pm 0.130) \times 10^{-1}$
II		0.300 ± 0.012	0.328 ± 0.004	8.478 ± 0.112	$(7.419 \pm 0.180) \times 10^{-1}$	15/12
III		0.300 ± 0.014	0.306 ± 0.002	8.301 ± 0.091	$(5.999 \pm 0.100) \times 10^{-1}$	7/12
IV		0.300 ± 0.008	0.287 ± 0.003	7.782 ± 0.093	$(5.099 \pm 0.150) \times 10^{-1}$	7/12
V		0.300 ± 0.011	0.270 ± 0.002	7.355 ± 0.043	$(4.500 \pm 0.050) \times 10^{-1}$	5/12
VI		0.300 ± 0.022	0.257 ± 0.001	7.351 ± 0.052	$(3.669 \pm 0.080) \times 10^{-1}$	10/12
VII		0.300 ± 0.019	0.223 ± 0.002	6.553 ± 0.063	$(3.060 \pm 0.049) \times 10^{-1}$	8/12
VIII		0.300 ± 0.014	0.213 ± 0.003	6.554 ± 0.081	$(2.339 \pm 0.040) \times 10^{-1}$	7/12
IX		0.300 ± 0.012	0.192 ± 0.001	6.456 ± 0.043	$(1.560 \pm 0.040) \times 10^{-1}$	10/12
X		0.300 ± 0.025	0.152 ± 0.001	6.000 ± 0.019	$(6.899 \pm 0.026) \times 10^{-2}$	15/12
$\Xi^- + \bar{\Xi}^+$ ($ssd, \bar{s}\bar{s}\bar{d}$) $(1/N_{evt})d^2N/dp_T dy$ [(GeV/c) $^{-1}$]	I	0.255 ± 0.008	0.431 ± 0.002	10.059 ± 0.048	$(1.299 \pm 0.013) \times 10^{-1}$	6/9
	II	0.255 ± 0.007	0.405 ± 0.003	10.013 ± 0.093	$(9.600 \pm 0.140) \times 10^{-2}$	5/9
	III	0.255 ± 0.013	0.381 ± 0.003	9.603 ± 0.190	$(7.599 \pm 0.219) \times 10^{-2}$	9/9
	IV	0.255 ± 0.011	0.371 ± 0.002	9.590 ± 0.112	$(6.099 \pm 0.120) \times 10^{-2}$	6/9
	V	0.255 ± 0.021	0.353 ± 0.003	9.558 ± 0.170	$(5.399 \pm 0.140) \times 10^{-2}$	14/9
	VI	0.255 ± 0.012	0.339 ± 0.002	9.557 ± 0.087	$(4.299 \pm 0.130) \times 10^{-2}$	14/9
	VII	0.255 ± 0.013	0.317 ± 0.002	8.985 ± 0.152	$(3.199 \pm 0.080) \times 10^{-2}$	12/9
	VIII	0.255 ± 0.007	0.280 ± 0.002	8.000 ± 0.122	$(2.600 \pm 0.070) \times 10^{-2}$	13/9
	IX	0.255 ± 0.004	0.242 ± 0.001	6.593 ± 0.088	$(1.600 \pm 0.010) \times 10^{-2}$	4/9
	X	0.255 ± 0.012	0.201 ± 0.002	6.587 ± 0.080	$(5.900 \pm 0.160) \times 10^{-3}$	7/9
$\Omega^- + \bar{\Omega}^+$ ($sss, \bar{s}\bar{s}\bar{s}$) $(1/N_{evt})d^2N/dp_T dy$ [(GeV/c) $^{-1}$]	I+II	0.830 ± 0.021	0.335 ± 0.001	9.656 ± 0.013	$(1.020 \pm 0.003) \times 10^{-2}$	1/2
	III+IV	0.830 ± 0.018	0.290 ± 0.001	9.640 ± 0.013	$(4.100 \pm 0.200) \times 10^{-3}$	5/2
	V+VI	0.830 ± 0.020	0.288 ± 0.001	9.640 ± 0.016	$(4.099 \pm 0.150) \times 10^{-3}$	4/2
	VII+VIII	0.830 ± 0.004	0.276 ± 0.002	9.640 ± 0.008	$(1.9000 \pm 0.080) \times 10^{-3}$	8/2
	IX+X	0.830 ± 0.022	0.233 ± 0.003	9.622 ± 0.008	$(6.299 \pm 0.150) \times 10^{-4}$	1/1

sion of p_T distribution is not available, the Monte Carlo method is performed in the calculations. As we know, for a wide p_T range, there are at least two components namely the soft and hard components in the structure of p_T spectrum. The present work shows that we do not need to distinguish the two components. Instead, we may use a set of parameters to fit a wide p_T spectrum, though the parameters are multi-factor dependent.

B. Tendencies of parameters

In order to see more intuitively the dependence of parameters on the centrality C (the multiplicity is converted to centrality in pp collisions), rest mass m_0 of the hadron, and constituent mass m_q of the quark, we show the multi-factor dependent parameters in Figures 5–12, where the values of parameters are cited in Tables 1–4.

Table 3. Values of a_0 , T , n , N_0 , χ^2 , and ndof corresponding to the curves in Figure 3 for p-Pb collisions at $\sqrt{s_{NN}} = 5.02$ TeV. The particle type (quark structure), spectrum form, and centrality are given together.

Particle (quark structure) spectrum form	Centrality	a^0	T (GeV)	n	N_0	χ^2/ndof
$\pi^+ + \pi^-$ ($u\bar{d}, d\bar{u}$) $(1/N_{evt}2\pi p_T)d^2N/dp_T dy$ [[GeV/c] ⁻²]	0-5%	-0.550 ± 0.003	0.382 ± 0.003	6.244 ± 0.063	$(2.130 \pm 0.025) \times 10^1$	148/54
	5-10%	-0.550 ± 0.004	0.370 ± 0.002	6.004 ± 0.072	$(1.743 \pm 0.028) \times 10^1$	135/54
	10-20%	-0.550 ± 0.004	0.358 ± 0.001	5.619 ± 0.121	$(1.461 \pm 0.025) \times 10^1$	148/54
	20-40%	-0.550 ± 0.005	0.344 ± 0.001	5.616 ± 0.030	$(1.153 \pm 0.019) \times 10^1$	142/54
	40-60%	-0.550 ± 0.004	0.317 ± 0.002	5.330 ± 0.034	$(8.168 \pm 0.251) \times 10^0$	130/54
	60-80%	-0.550 ± 0.002	0.300 ± 0.002	5.332 ± 0.033	$(5.027 \pm 0.094) \times 10^0$	93/54
80-100%	-0.550 ± 0.003	0.255 ± 0.001	5.032 ± 0.038	$(2.199 \pm 0.072) \times 10^0$	173/54	
$K^+ + K^-$ ($u\bar{s}, s\bar{u}$) $(1/N_{evt}2\pi p_T)d^2N/dp_T dy$ [[GeV/c] ⁻²]	0-5%	0.220 ± 0.007	0.265 ± 0.002	5.968 ± 0.021	$(2.859 \pm 0.060) \times 10^0$	63/47
	5-10%	0.220 ± 0.013	0.260 ± 0.004	5.948 ± 0.083	$(2.356 \pm 0.063) \times 10^0$	36/47
	10-20%	0.220 ± 0.006	0.254 ± 0.002	5.872 ± 0.061	$(1.948 \pm 0.038) \times 10^0$	24/47
	20-40%	0.220 ± 0.006	0.253 ± 0.002	5.878 ± 0.046	$(1.477 \pm 0.025) \times 10^0$	11/47
	40-60%	0.220 ± 0.003	0.241 ± 0.001	5.741 ± 0.053	$(9.990 \pm 0.031) \times 10^{-1}$	28/47
	60-80%	0.220 ± 0.006	0.216 ± 0.003	5.446 ± 0.048	$(5.969 \pm 0.157) \times 10^{-1}$	32/47
80-100%	0.220 ± 0.007	0.190 ± 0.002	5.446 ± 0.056	$(2.419 \pm 0.062) \times 10^{-1}$	88/47	
$p + \bar{p}$ ($uud, \bar{u}\bar{u}\bar{d}$) $(1/N_{evt}2\pi p_T)d^2N/dp_T dy$ [[GeV/c] ⁻²]	0-5%	0.398 ± 0.021	0.283 ± 0.003	8.270 ± 0.063	$(2.262 \pm 0.075) \times 10^0$	56/45
	5-10%	0.398 ± 0.012	0.274 ± 0.002	8.155 ± 0.120	$(1.847 \pm 0.062) \times 10^0$	34/45
	10-20%	0.398 ± 0.024	0.267 ± 0.004	7.900 ± 0.111	$(1.558 \pm 0.037) \times 10^0$	33/45
	20-40%	0.398 ± 0.021	0.256 ± 0.004	7.885 ± 0.112	$(1.206 \pm 0.019) \times 10^0$	18/45
	40-60%	0.398 ± 0.024	0.236 ± 0.004	7.652 ± 0.052	$(8.357 \pm 0.125) \times 10^{-1}$	36/45
	60-80%	0.398 ± 0.029	0.208 ± 0.003	7.145 ± 0.066	$(5.152 \pm 0.144) \times 10^{-1}$	45/45
K_S^0 ($d\bar{s}$) $(1/N_{evt}2\pi p_T)d^2N/dp_T dy$ [[GeV/c] ⁻²]	0-5%	0.220 ± 0.005	0.279 ± 0.002	6.451 ± 0.052	$(1.445 \pm 0.028) \times 10^0$	13/30
	5-10%	0.220 ± 0.007	0.279 ± 0.003	6.436 ± 0.068	$(1.162 \pm 0.028) \times 10^0$	14/30
	10-20%	0.220 ± 0.010	0.278 ± 0.002	6.426 ± 0.049	$(9.581 \pm 0.157) \times 10^{-1}$	18/30
	20-40%	0.220 ± 0.008	0.260 ± 0.002	6.000 ± 0.062	$(7.383 \pm 0.219) \times 10^{-1}$	20/30
	40-60%	0.220 ± 0.010	0.244 ± 0.002	5.762 ± 0.061	$(5.027 \pm 0.126) \times 10^{-1}$	21/30
	60-80%	0.220 ± 0.013	0.217 ± 0.001	5.527 ± 0.058	$(3.079 \pm 0.072) \times 10^{-1}$	45/30
80-100%	0.220 ± 0.011	0.181 ± 0.002	5.125 ± 0.059	$(1.319 \pm 0.053) \times 10^{-1}$	33/30	
$\Sigma(1385)^+(suu)$ $(1/N_{evt}2\pi p_T)d^2N/dp_T dy$ [[GeV/c] ⁻²]	0-20%	1.300 ± 0.006	0.201 ± 0.002	7.682 ± 0.065	$(4.441 \pm 0.050) \times 10^{-2}$	2/2
	20-60%	1.300 ± 0.004	0.183 ± 0.001	7.661 ± 0.056	$(2.396 \pm 0.035) \times 10^{-2}$	4/2
	60-100%	1.300 ± 0.008	0.157 ± 0.002	7.523 ± 0.077	$(6.596 \pm 0.035) \times 10^{-3}$	9/2
$\Lambda + \bar{\Lambda}$ ($uds, \bar{u}\bar{d}\bar{s}$) $(1/N_{evt}2\pi p_T)d^2N/dp_T dy$ [[GeV/c] ⁻²]	0-5%	1.300 ± 0.010	0.187 ± 0.001	8.512 ± 0.058	$(8.167 \pm 0.220) \times 10^{-1}$	3/16
	5-10%	1.300 ± 0.010	0.181 ± 0.001	8.187 ± 0.055	$(6.439 \pm 0.094) \times 10^{-1}$	4/16
	10-20%	1.300 ± 0.011	0.174 ± 0.003	7.949 ± 0.063	$(5.403 \pm 0.063) \times 10^{-1}$	2/16
	20-40%	1.300 ± 0.005	0.165 ± 0.001	7.731 ± 0.052	$(4.083 \pm 0.037) \times 10^{-1}$	4/16
	40-60%	1.300 ± 0.018	0.154 ± 0.003	7.631 ± 0.089	$(2.764 \pm 0.069) \times 10^{-1}$	12/16
	60-80%	1.300 ± 0.023	0.131 ± 0.002	6.958 ± 0.083	$(1.633 \pm 0.041) \times 10^{-1}$	10/16
80-100%	1.300 ± 0.019	0.111 ± 0.002	6.692 ± 0.102	$(6.283 \pm 0.251) \times 10^{-2}$	18/16	
$(\Xi^- + \bar{\Xi}^+)/2$ ($ssd, \bar{s}\bar{s}\bar{d}$) $(1/N_{evt}2\pi p_T)d^2N/dp_T dy$ [[GeV/c] ⁻²]	0-5%	1.000 ± 0.031	0.259 ± 0.003	9.399 ± 0.102	$(5.781 \pm 0.079) \times 10^{-2}$	13/13
	5-10%	1.000 ± 0.019	0.249 ± 0.004	8.964 ± 0.103	$(4.618 \pm 0.110) \times 10^{-2}$	9/13
	10-20%	1.000 ± 0.018	0.244 ± 0.003	8.882 ± 0.089	$(3.770 \pm 0.085) \times 10^{-2}$	7/13
	20-40%	1.000 ± 0.007	0.235 ± 0.001	8.824 ± 0.086	$(2.733 \pm 0.050) \times 10^{-2}$	6/13
	40-60%	1.000 ± 0.023	0.222 ± 0.002	8.819 ± 0.079	$(1.791 \pm 0.053) \times 10^{-2}$	11/13
	60-80%	1.000 ± 0.002	0.203 ± 0.001	8.030 ± 0.001	$(9.204 \pm 0.003) \times 10^{-3}$	40/12
80-100%	1.000 ± 0.000	0.153 ± 0.000	6.324 ± 0.001	$(3.299 \pm 0.003) \times 10^{-3}$	11/11	
$(\Omega^- + \bar{\Omega}^+)/2$ ($sss, \bar{s}\bar{s}\bar{s}$) $(1/N_{evt}2\pi p_T)d^2N/dp_T dy$ [[GeV/c] ⁻²]	0-5%	0.830 ± 0.008	0.319 ± 0.002	8.346 ± 0.062	$(6.597 \pm 0.087) \times 10^{-3}$	4/4
	5-10%	0.830 ± 0.006	0.319 ± 0.002	8.139 ± 0.088	$(5.655 \pm 0.094) \times 10^{-3}$	3/4
	10-20%	0.830 ± 0.021	0.294 ± 0.004	7.722 ± 0.103	$(4.398 \pm 0.069) \times 10^{-3}$	7/4
	20-40%	0.830 ± 0.021	0.278 ± 0.002	7.233 ± 0.111	$(3.047 \pm 0.038) \times 10^{-3}$	2/4
	40-60%	0.830 ± 0.008	0.243 ± 0.003	6.832 ± 0.193	$(1.885 \pm 0.063) \times 10^{-3}$	7/4
	60-80%	0.830 ± 0.011	0.234 ± 0.002	6.901 ± 0.098	$(1.005 \pm 0.019) \times 10^{-2}$	5/4
80-100%	0.830 ± 0.010	0.192 ± 0.003	6.998 ± 0.197	$(3.994 \pm 0.016) \times 10^{-4}$	2/4	

Table 4. Values of a^0 , T , n , N_0 , χ^2 , and ndof corresponding to the curves in Figure 4 for Pb–Pb collisions at $\sqrt{s_{NN}} = 2.76$ TeV. The particle type (quark structure), spectrum form, and centrality are given together.

Particle (quark structure) spectrum form	Centrality	a_0	T (GeV)	n	N_0	χ^2/ndof
$\pi^+ + \pi^-$ ($u\bar{d}, d\bar{u}$) ($1/N_{evt}2\pi p_T)d^2N/dp_T dy$ [(GeV/c) $^{-2}$]	0–5%	-0.300 ± 0.004	0.236 ± 0.001	6.599 ± 0.012	$(2.325 \pm 0.042) \times 10^3$	562/59
	5–10%	-0.300 ± 0.002	0.236 ± 0.002	6.506 ± 0.014	$(1.930 \pm 0.021) \times 10^3$	469/59
	10–20%	-0.300 ± 0.004	0.236 ± 0.002	6.226 ± 0.023	$(1.414 \pm 0.040) \times 10^3$	471/59
	20–40%	-0.300 ± 0.005	0.237 ± 0.002	6.206 ± 0.022	$(8.043 \pm 0.302) \times 10^2$	331/59
	40–60%	-0.300 ± 0.004	0.225 ± 0.002	5.850 ± 0.025	$(3.086 \pm 0.101) \times 10^2$	158/59
	60–80%	-0.300 ± 0.009	0.218 ± 0.004	5.668 ± 0.026	$(8.193 \pm 0.367) \times 10^1$	99/59
$K^+ + K^-$ ($u\bar{s}, s\bar{u}$) ($1/N_{evt}2\pi p_T)d^2N/dp_T dy$ [(GeV/c) $^{-2}$]	0–5%	0.300 ± 0.008	0.222 ± 0.002	7.198 ± 0.031	$(3.177 \pm 0.093) \times 10^2$	607/54
	5–10%	0.300 ± 0.009	0.221 ± 0.001	7.178 ± 0.025	$(2.724 \pm 0.070) \times 10^2$	524/54
	10–20%	0.300 ± 0.014	0.216 ± 0.003	6.926 ± 0.028	$(2.161 \pm 0.058) \times 10^2$	415/54
	20–40%	0.300 ± 0.022	0.211 ± 0.003	6.526 ± 0.032	$(1.190 \pm 0.035) \times 10^2$	291/54
	40–60%	0.300 ± 0.012	0.202 ± 0.005	6.157 ± 0.040	$(4.363 \pm 0.151) \times 10^1$	95/54
	60–80%	0.300 ± 0.009	0.201 ± 0.003	6.102 ± 0.026	$(1.116 \pm 0.035) \times 10^1$	25/54
$p + \bar{p}$ ($uud, \bar{u}\bar{u}\bar{d}$) ($1/N_{evt}2\pi p_T)d^2N/dp_T dy$ [(GeV/c) $^{-2}$]	0–5%	1.000 ± 0.005	0.209 ± 0.003	10.357 ± 0.023	$(1.089 \pm 0.050) \times 10^2$	490/45
	5–10%	1.000 ± 0.020	0.207 ± 0.002	10.337 ± 0.035	$(9.178 \pm 0.402) \times 10^1$	444/45
	10–20%	1.000 ± 0.015	0.205 ± 0.002	10.077 ± 0.080	$(6.977 \pm 0.312) \times 10^1$	374/45
	20–40%	1.000 ± 0.019	0.193 ± 0.004	9.391 ± 0.100	$(3.921 \pm 0.090) \times 10^1$	259/45
	40–60%	1.000 ± 0.003	0.170 ± 0.003	8.183 ± 0.082	$(1.553 \pm 0.060) \times 10^1$	104/45
	60–80%	1.000 ± 0.002	0.155 ± 0.002	8.005 ± 0.007	$(4.524 \pm 0.090) \times 10^0$	14/45
K_S^0 ($d\bar{s}$) ($1/N_{evt}d^2N/dp_T dy$ [(GeV/c) $^{-2}$]	0–5%	0.220 ± 0.033	0.251 ± 0.005	8.022 ± 0.012	$(1.003 \pm 0.050) \times 10^2$	545/29
	5–10%	0.220 ± 0.022	0.251 ± 0.005	8.018 ± 0.017	$(8.660 \pm 0.340) \times 10^1$	406/29
	10–20%	0.220 ± 0.018	0.251 ± 0.003	8.018 ± 0.068	$(6.930 \pm 0.300) \times 10^1$	317/29
	20–40%	0.220 ± 0.012	0.239 ± 0.004	7.238 ± 0.053	$(3.889 \pm 0.179) \times 10^1$	229/29
	40–60%	0.220 ± 0.013	0.222 ± 0.002	6.490 ± 0.049	$(1.469 \pm 0.056) \times 10^1$	61/29
	60–80%	0.220 ± 0.008	0.214 ± 0.002	6.083 ± 0.040	$(3.579 \pm 0.039) \times 10^0$	19/29
	80–90%	0.220 ± 0.009	0.195 ± 0.002	5.719 ± 0.067	$(7.959 \pm 0.219) \times 10^{-1}$	22/28
$(K^{*0} + \bar{K}^{*0})/2$ ($u\bar{s}, s\bar{u}$) ($1/N_{evt}d^2N/dp_T dy$ [(GeV/c) $^{-1}$]	0–5%	1.950 ± 0.009	0.156 ± 0.004	8.468 ± 0.064	$(1.728 \pm 0.094) \times 10^1$	29/9
	5–10%	1.950 ± 0.031	0.148 ± 0.003	8.276 ± 0.061	$(1.521 \pm 0.125) \times 10^1$	23/9
	10–20%	1.950 ± 0.040	0.148 ± 0.003	7.978 ± 0.105	$(1.175 \pm 0.157) \times 10^1$	50/9
	20–30%	1.950 ± 0.026	0.144 ± 0.005	7.646 ± 0.203	$(8.734 \pm 0.817) \times 10^0$	32/9
	30–40%	1.950 ± 0.019	0.140 ± 0.002	7.646 ± 0.104	$(6.723 \pm 0.565) \times 10^0$	13/9
	40–50%	1.950 ± 0.018	0.138 ± 0.002	7.613 ± 0.066	$(4.398 \pm 0.163) \times 10^0$	7/9
Λ (uds) ($1/N_{evt}d^2N/dp_T dy$ [(GeV/c) $^{-1}$]	0–5%	2.600 ± 0.014	0.125 ± 0.002	11.456 ± 0.015	$(2.403 \pm 0.060) \times 10^1$	84/27
	5–10%	2.600 ± 0.012	0.124 ± 0.001	11.406 ± 0.013	$(2.170 \pm 0.060) \times 10^1$	43/27
	10–20%	2.600 ± 0.013	0.127 ± 0.002	11.406 ± 0.021	$(1.740 \pm 0.090) \times 10^1$	30/27
	20–40%	2.600 ± 0.008	0.110 ± 0.001	9.993 ± 0.033	$(9.899 \pm 0.299) \times 10^0$	25/27
	40–60%	2.600 ± 0.006	0.100 ± 0.001	9.367 ± 0.045	$(3.700 \pm 0.079) \times 10^0$	5/27
	60–80%	2.600 ± 0.014	0.085 ± 0.001	8.383 ± 0.057	$(8.800 \pm 0.099) \times 10^{-1}$	21/27
	80–90%	2.600 ± 0.023	0.078 ± 0.001	8.169 ± 0.062	$(1.720 \pm 0.069) \times 10^{-1}$	37/25
$(\Xi^- + \bar{\Xi}^+)/2$ ($ssd, \bar{s}\bar{s}\bar{d}$) ($1/N_{evt}d^2N/dp_T dy$ [(GeV/c) $^{-1}$]	0–10%	1.955 ± 0.008	0.194 ± 0.002	16.514 ± 0.018	$(3.390 \pm 0.099) \times 10^0$	68/23
	10–20%	1.955 ± 0.010	0.181 ± 0.001	14.343 ± 0.089	$(2.579 \pm 0.059) \times 10^0$	18/23
	20–40%	1.955 ± 0.014	0.168 ± 0.001	12.385 ± 0.103	$(1.460 \pm 0.039) \times 10^0$	21/23
	40–60%	1.955 ± 0.014	0.164 ± 0.002	12.152 ± 0.100	$(4.850 \pm 0.159) \times 10^{-1}$	27/21
	60–80%	1.955 ± 0.025	0.130 ± 0.002	9.000 ± 0.013	$(1.099 \pm 0.019) \times 10^{-1}$	18/21
$(\Omega^- + \bar{\Omega}^+)/2$ ($sss, \bar{s}\bar{s}\bar{s}$) ($1/N_{evt}d^2N/dp_T dy$ [(GeV/c) $^{-1}$]	0–10%	2.150 ± 0.009	0.186 ± 0.002	12.707 ± 0.048	$(5.500 \pm 0.099) \times 10^{-1}$	6/9
	10–20%	2.150 ± 0.008	0.179 ± 0.002	12.492 ± 0.056	$(4.099 \pm 0.109) \times 10^{-1}$	8/9
	20–40%	2.150 ± 0.008	0.176 ± 0.002	12.400 ± 0.088	$(2.280 \pm 0.140) \times 10^{-1}$	10/9
	40–60%	2.150 ± 0.011	0.138 ± 0.001	9.008 ± 0.066	$(7.599 \pm 0.129) \times 10^{-2}$	3/8
	60–80%	2.150 ± 0.014	0.136 ± 0.002	9.032 ± 0.101	$(1.299 \pm 0.100) \times 10^{-2}$	7/6

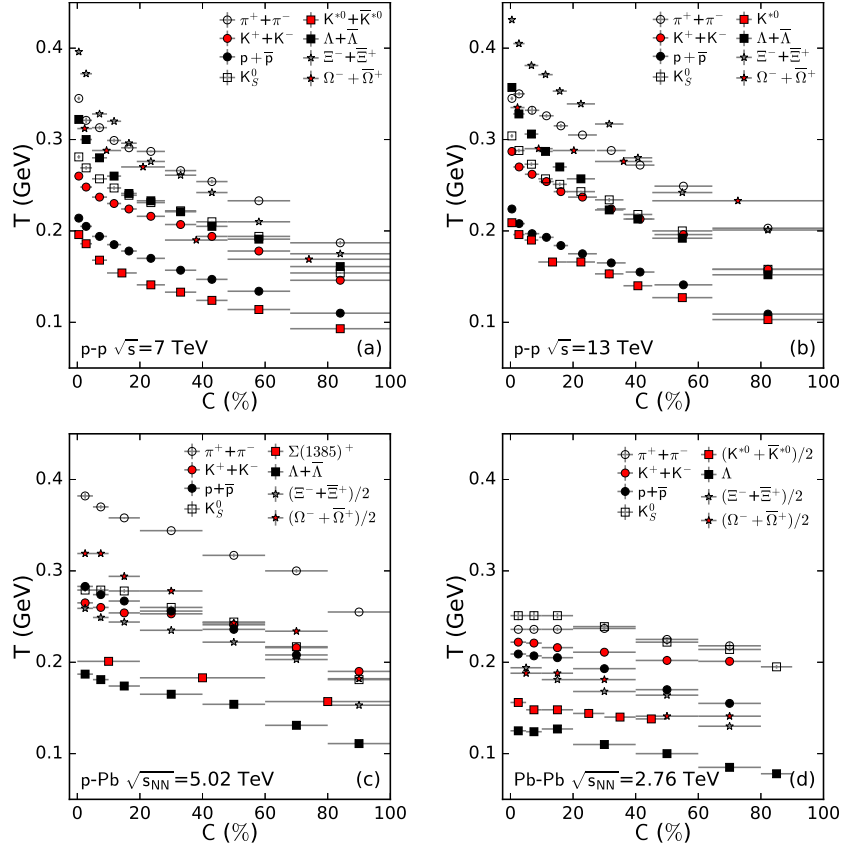


Fig. 5. Dependence of T on C for pp collisions at $\sqrt{s} = 7$ TeV (a), pp collisions at $\sqrt{s} = 13$ TeV (b), p -Pb collisions at $\sqrt{s_{NN}} = 5.02$ TeV (c), and Pb-Pb collisions at $\sqrt{s_{NN}} = 2.76$ TeV (d). Different symbols represent the parameters from the p_T spectra of different particles marked in the panels.

Because of the revised index a_0 being independent of the centrality, we have not shown the plot for the centrality dependent a_0 .

Figures 5 and 6 show the dependence of effective temperature T and entropy-related index n on centrality C respectively. Panels (a–d) are for pp collisions at $\sqrt{s} = 7$ TeV, pp collisions at $\sqrt{s} = 13$ TeV, p -Pb collisions at $\sqrt{s_{NN}} = 5.02$ TeV, and Pb-Pb collisions at $\sqrt{s_{NN}} = 2.76$ TeV, respectively. Different symbols represent the parameters from the p_T spectra of different particles marked in the panels. One can see that with the decrease of centrality from central to peripheral collisions, T and n decrease in most of the cases. Central collisions create higher concentration of energies because of larger number of participants and hence a higher system temperature, T is expected. As a consequence, this is expected to create a more thermalized system leading to larger value of n or smaller entropy index q , as $n = 1/(q - 1)$. These results are consistent with the fact that more central is the

collision, the system has a higher tendency of creating a high temperature thermalized system.

This result is consistent with our previous work [39] which also shows that T in central collisions is larger. In Ref. [39] we have studied the light (also including strangeness) and heavy particles produced in small system (pp , d -Au, and p -Pb collisions) and large system (Au-Au and Pb-Pb collisions) in the case of \mathbf{p}_{ti} being parallel. This result is also consistent with our another work published recently [62], which analyzes the kinetic freeze-out temperature T_0 extracted from narrow p_T spectra ($p_T < 4.5$ GeV/ c) of identified particles (π^+ , K^+ , p , K_S^0 , Λ , Ξ , $\Omega + \bar{\Omega}$) produced in copper-copper (Cu-Cu), Au-Au, and Pb-Pb collisions by the blast-wave model. That result shows larger T_0 in central collisions.

Figures 7–9 show the dependences of parameters a_0 , T , and n on the rest mass m_0 of particle, respectively. Same as Figures 5 and 6, panels (a–d) are for pp collisions at $\sqrt{s} = 7$ TeV, pp collisions at $\sqrt{s} = 13$ TeV, p -

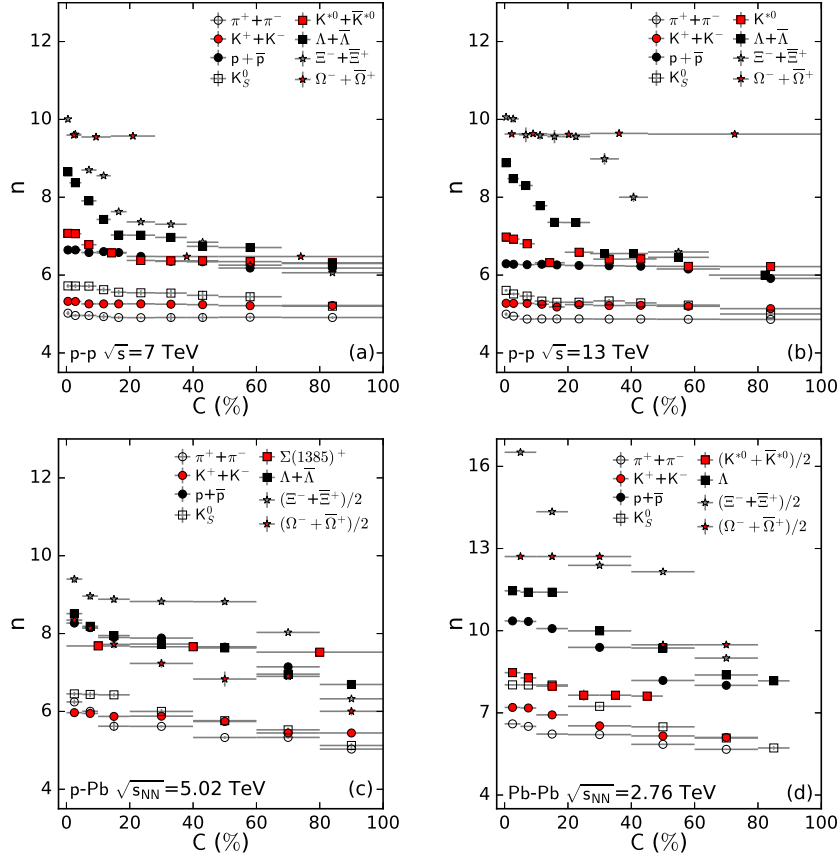


Fig. 6. Same as Figure 5, but showing the dependence of n on C .

Pb collisions at $\sqrt{s_{NN}} = 5.02$ TeV, and Pb–Pb collisions at $\sqrt{s_{NN}} = 2.76$ TeV, respectively. Different symbols represent the parameters from the p_T spectra of different particles marked in the panels. With the increase of m_0 , one can see that a_0 and n increases significantly for the four cases, and the tendency of T is strange: T decreases firstly and then increases, the boundary is at around $m_0 = 1$ GeV/ c^2 .

The results of the m_0 dependent parameters are not contradictory to our previous work [39] if we examine minutely the parameter plots around $m_0 = 1$ GeV/ c^2 there, though in which the analysis was done for a special case. The amplitudes of the m_0 dependent parameters in Figures 7–9 are different for the four cases. These differences are explained by different collision energies and system sizes. In particular, in Pb–Pb collisions, multiple scattering of particles in hot and dense matter affects the parameters. This multiple scattering also reflects the shadowing effect in which the subsequent medium has no chance to be collided due to the change of direction of motion of the particles in the multiple scattering.

The dependences of parameters a_0 , T , and n on the constituent mass m_q of quark are given in Figures 10–12, respectively. Same as Figures 5–9, panels (a–d) are for pp collisions at $\sqrt{s} = 7$ and 13 TeV, p –Pb collisions at $\sqrt{s_{NN}} = 5.02$ TeV, and Pb–Pb collisions at $\sqrt{s_{NN}} = 2.76$ TeV, respectively. Different symbols represent the parameters from the p_T spectra of different particles marked in the panels. One can see nearly the same parameters for m_u (m_d) and m_s , and some differences for the four collisions.

The present work on m_q dependent parameters is not contradictory to our previous work [39], though two more quarks (charm and bottom) are included there. The nearly the same parameters are observed due to very small difference between m_u (m_d) and m_s ($m_u = m_d = 0.31$ GeV/ c^2 and $m_s = 0.5$ GeV/ c^2 [60]). The differences in amplitudes for the four collisions are explained by different collision energies and system sizes, in particular by different system sizes, where the influence of multiple scattering in large system is considerable, as the explanations for Figures 7–9.

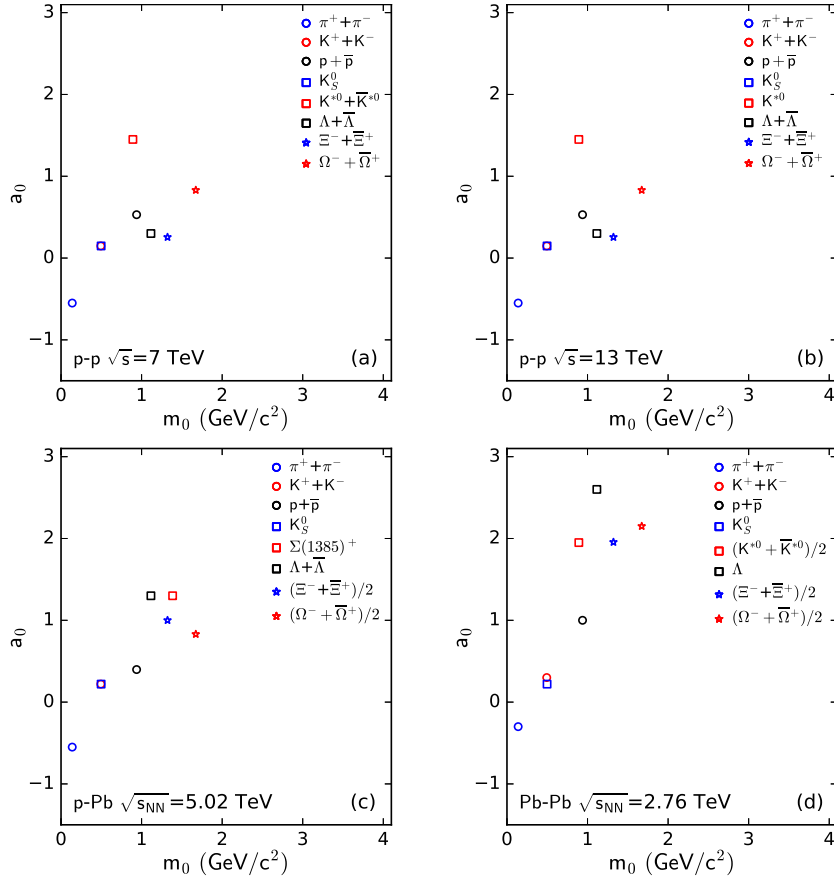


Fig. 7. Same as Figure 5, but showing the dependence of a_0 on m_0 .

C. Further discussion

The values of revised index a_0 extracted from the p_T spectra of $\pi^+ + \pi^-$ are negative, which means the upward tendency of the spectra in low- p_T region [38]. This is contributed by the resonance decays. The values of a_0 extracted from the p_T spectra of other particles are positive or even larger than 1, which means the downward tendency of the spectra in low- p_T region. This is caused by the constraints in the production of other particles. Larger constraint seems to be observed for strange particles/quark. Due to the limitation of normalization, any upward or downward tendency in low- p_T region will cause the shape change of the curve in intermediate- and high- p_T regions.

The values of effective temperature T extracted from the present work contain both the contributions of thermal motion and collective flow, which shows that T is larger than 0.2 GeV even 0.3 GeV. To dissociate the two contributions and obtain the kinetic freeze-out temperature T_0 and transverse flow velocity β_T , one has to apply

different methods which shows some level of inconsistencies in some cases. These inconsistencies mainly show in different centrality and size dependent behaviour of T_0 and β_T . In our opinion, T displays the coincident results and should be paid more attention. To obtain T_0 and β_T , a uniform method is needed at the first place. This issue is beyond the focus of the present work. In all cases, the entropy-related index $n > 4$ which means that $q < 1.25$, as expected for high-energy collisions. This is a q close to 1 and implies that the system at the quark level is in approximate equilibrium or local equilibrium.

As an extension of the special (parallel) case to general (arbitrary) one, the results from our previous work [38, 39] are confirmed more broadly here. Combining with our previous work, we may infer that the method used in the present work is suitable for wide ranges of collision energy, system size, event centrality, and particle species. Although the analytical expression of p_T distribution for the special case can be obtained, we may use the Monte Carlo method to calculate the p_T distribution for the general case.

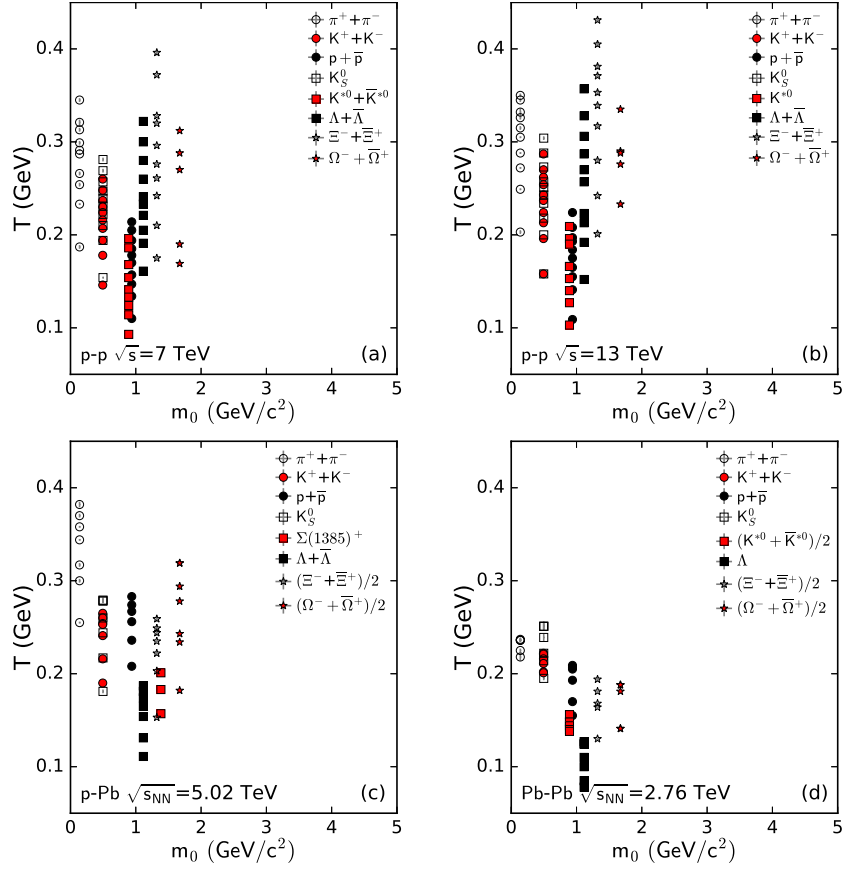


Fig. 8. Same as Figure 5, but showing the dependence of T on m_0 .

We note that the fit for the p_T spectra in Pb–Pb collisions is not good, in particular for the spectra in high- p_T region in central collisions. This is explained by the influence of multiple scattering of produced particles in hot and dense matter. To include the influence of multiple scattering, except for the superposition of the contributions of quarks with the TP-like form of transverse momenta and isotropic azimuths, we may need another function in the present framework. Or, we may use a two-component function to fit the p_T spectra in Pb–Pb collisions, where the second component can describe the contribution of multiple scattering.

The present work includes the contributions of soft excitations and hard scattering processes together, without having a scope to separate them in the ambient of the present analysis of identified particle transverse momentum spectra using TP-like distribution function. The possible departure of the fit from the data in high- p_T region in central Pb–Pb collisions could be due to multiple scatterings and medium effects and in addition, a thermalized medium being formed in these nuclear collisions.

IV. SUMMARY AND CONCLUSIONS

The present analysis is summarized below with important observations and conclusions.

(a) The transverse momentum, p_T spectra of various light hadrons (including some strange particles) produced in pp collisions at $\sqrt{s} = 7$ and 13 TeV, p -Pb collisions at $\sqrt{s_{NN}} = 5.02$ GeV, and Pb–Pb collisions at $\sqrt{s_{NN}} = 2.76$ TeV for different multiplicity or centrality classes have been studied in the framework of a multi-source thermal model at the quark level. The contribution of each constituent quark to hadron's p_T is assumed to obey the TP-like function with isotropic azimuth. The calculations are performed by Monte Carlo method and compared with the experimental data measured by the ALICE Collaboration. A reasonably good description of the spectra across various collision species and energies available at the LHC is observed.

(b) With the decrease of final state multiplicity from central to peripheral collisions, the revised index, a_0 being nearly invariant, the effective temperature, T

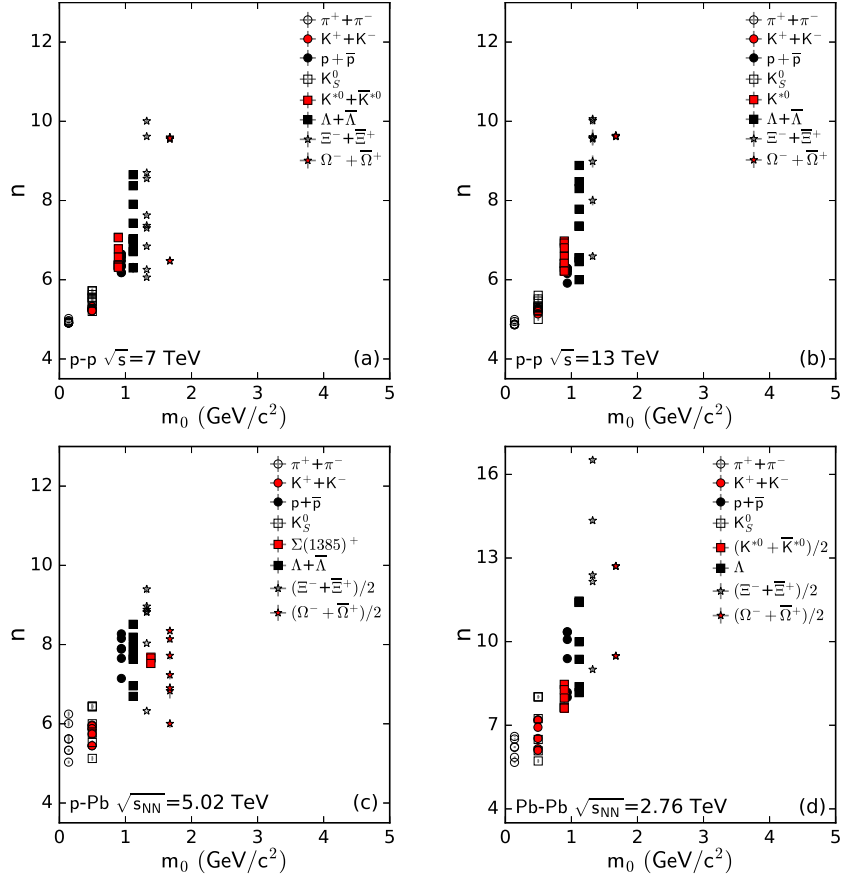


Fig. 9. Same as Figure 5, but showing the dependence of n on m_0 .

and the entropy-related index, n decrease in most of the cases. With the increase of the rest mass m_0 of the particles, a_0 and n increases significantly, and T decreases first and then increases with the boundary being at around $1 \text{ GeV}/c^2$. Higher collision energy is deposited in central collisions, which results in larger T . The system in central collisions is closer to the equilibrium, which results in larger n or smaller entropy index, q . Both the soft excitation and hard scattering processes are considered uniformly. The influence of multiple scattering in large system is considerable.

Acknowledgments

The work of Pei-Pin Yang was supported by the China Scholarship Council (Chinese Government Scholarship) under Grant No. 202008140170, the Shanxi Provincial Innovative Foundation for Graduate Education under Grant No. 2019SY053, and the Innovative Foundation for Graduate Education of Shanxi University. The work of Shanxi Group was supported by the

National Natural Science Foundation of China under Grant Nos. 12047571, 11575103, and 11947418, the Scientific and Technological Innovation Programs of Higher Education Institutions in Shanxi (STIP) under Grant No. 201802017, the Shanxi Provincial Natural Science Foundation under Grant No. 201901D111043, and the Fund for Shanxi “1331 Project” Key Subjects Construction. Raghunath Sahoo acknowledges the financial supports under the CERN Scientific Associateship, CERN, Geneva, Switzerland and the financial grants under DAE-BRNS Project No. 58/14/29/2019-BRNS of Government of India.

Author Contributions All authors listed have made a substantial, direct, and intellectual contribution to the work and approved it for publication.

Data Availability Statement This manuscript has no associated data or the data will not be deposited. [Authors’ comment: The data used to support the findings of this study are included within the article and are cited at relevant places within the text as references.]

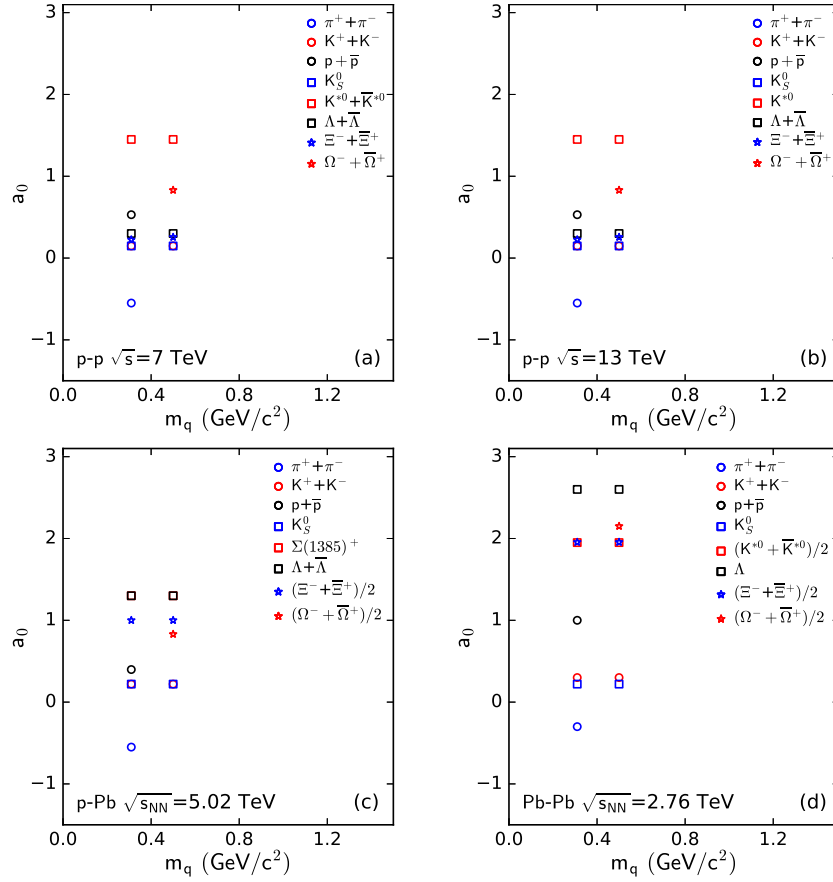


Fig. 10. Same as Figure 5, but showing the dependence of a_0 on m_q .

Ethical Approval The authors declare that they are in compliance with ethical standards regarding the content of this paper.

Disclosure The funding agencies have no role in the design of the study; in the collection, analysis, or interpretation of the data; in the writing of the

manuscript, or in the decision to publish the results.

Conflict of Interest The authors declare that there are no conflicts of interest regarding the publication of this paper.

-
- [1] J. Rafelski, B. Muller, Phys. Rev. Lett **48**, 1066 (1982).
 [2] P. Koch, and J. Rafelski, W. Greiner, Phys. Lett. B **123**, 151 (1983).
 [3] P. Koch, B. Muller, J. Rafelski, Phys. Rept. **142**, 167 (1986).
 [4] C. Blume, C. Markert, Prog. Part. Nucl. Phys. **66**, 834 (2011).
 [5] S. Forte, G. Watt, Ann. Rev. Nucl. Part. Sci. **63**, 291 (2013).
 [6] E. Andersen, et al. Phys. Lett. B **433**, 209 (1998).
 [7] STAR Collaboration (J. Adams et al.), Nucl. Phys. A **757**, 102 (2005).
 [8] CMS Collaboration (V. Khachatryan et al.), JHEP **2010**(09), 091 (2010).
 [9] CMS Collaboration (V. Khachatryan et al.), Phys. Lett. B **765**, 193 (2017).
 [10] ALICE Collaboration (B. B. Abelev et al.), Phys. Lett. B **728**, 25 (2014).
 [11] ALICE Collaboration (J. Adam et al.), Phys. Lett. B **758**, 389 (2016).
 [12] CMS Collaboration (S. Chatrchyan et al.), Phys. Lett. B **718**, 795 (2013).

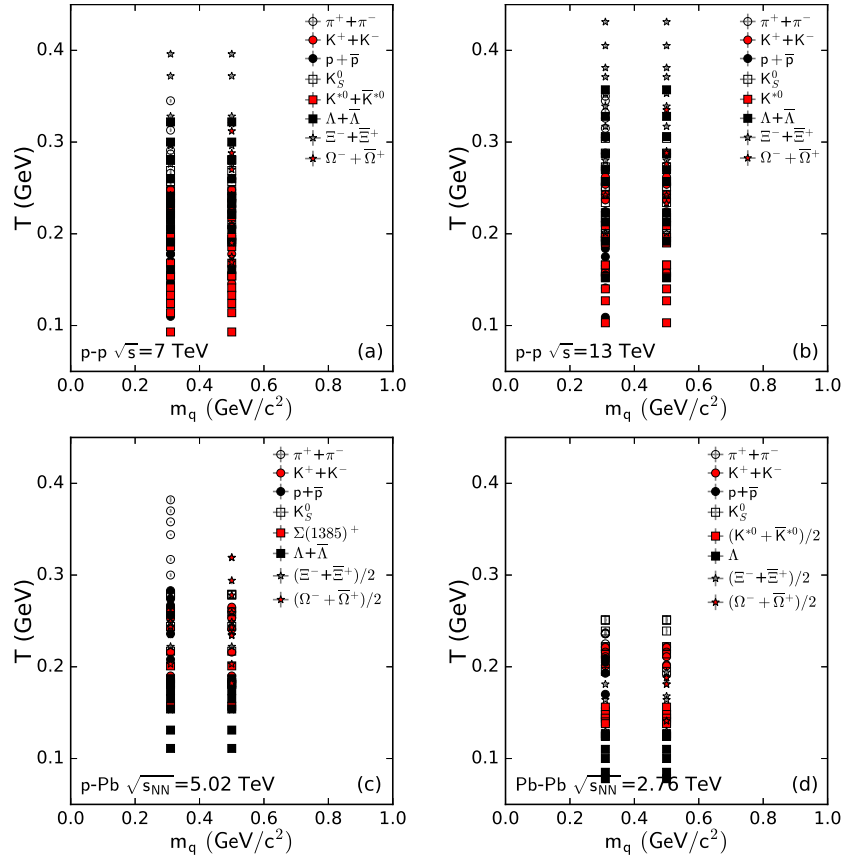


Fig. 11. Same as Figure 5, but showing the dependence of T on m_q .

- [13] ALICE Collaboration (B. Abelev et al.), Phys. Lett. B **719**, 29 (2013).
- [14] ATLAS Collaboration (G. Aad et al.), Phys. Rev. Lett. **110**, 182302 (2013).
- [15] ATLAS Collaboration (G. Aad et al.), Phys. Lett. B **725**, 60 (2013).
- [16] CMS Collaboration (S. Chatrchyan et al.), Phys. Lett. B **724**, 213 (2013).
- [17] ALICE Collaboration (B. Abelev et al.), Phys. Lett. B **726**, 164 (2013).
- [18] CMS Collaboration (V. Khachatryan et al.), Phys. Lett. B **768**, 103 (2017).
- [19] J. Rafelski, B. Muller, Phys. Rev. Lett. **48**, 1066 (1982).
- [20] STAR Collaboration (B. I. Abelev et al.), Phys. Rev. C **77**, 044908 (2008).
- [21] WA97 Collaboration (E. Andersen et al.), Phys. Lett. B **449**, 401 (1999).
- [22] STAR Collaboration (J. Adams et al.), Phys. Rev. Lett. **92**, 182301 (2004).
- [23] STAR Collaboration (J. Adams et al.), Nucl. Phys. A **757**, 102 (2005).
- [24] PHENIX Collaboration (K. Adcox et al.), Nucl. Phys. A **757**, 184 (2005).
- [25] ALICE Collaboration (B. B. Abelev et al.), Phys. Rev. C **90**, 054901 (2014).
- [26] ATLAS Collaboration (G. Aad, et al.) Phys. Rev. Lett. **116**, 172301 (2016).
- [27] ALICE Collaboration (S. Acharya et al.), Phys. Rev. Lett. **123**, 142301 (2019).
- [28] CMS Collaboration (V. Khachatryan et al.), Phys. Lett. B **765**, 193 (2017).
- [29] CMS Collaboration (V. Khachatryan et al.), Phys. Rev. Lett. **115**, 012301 (2015).
- [30] ATLAS Collaboration (M. Aaboud et al.), Eur. Phys. J. C **77**, 428 (2017).
- [31] ALICE Collaboration (S. Acharya et al.), Phys. Rev. C **99**, 024906 (2019).
- [32] ALICE Collaboration (J. Adam et al.), Nature Phys. **13**, 535 (2017).
- [33] C. Tsallis, J. Statist. Phys. **52**, 479 (1988).
- [34] T. S. Biro, G. Purcsel, K. Urmosy, Eur. Phys. J. A **40**, 325 (2009).
- [35] H. Zheng, L. L. Zhu, A. Bonasera, Phys. Rev. D **92**, 074009 (2015).
- [36] H. Zheng, L. L. Zhu, Adv. High Energy Phys. **2015**, 180491 (2015).

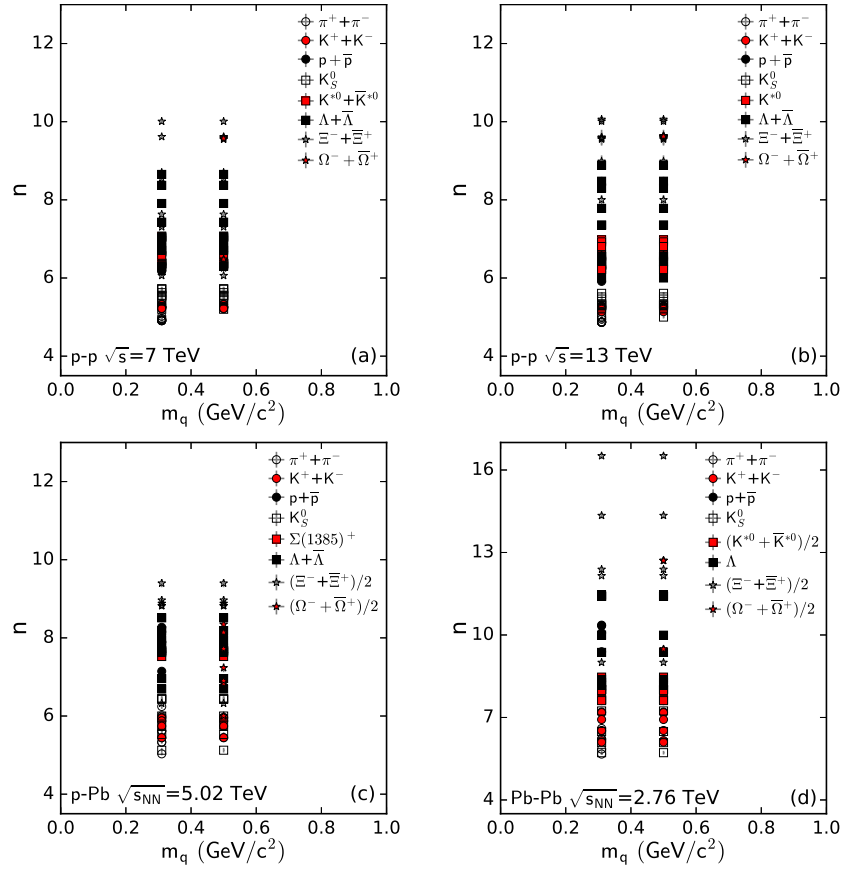


Fig. 12. Same as Figure 5, but showing the dependence of n on m_q

- [37] J. Cleymans, M. W. Paradza, *Physics* **2**, 654 (2020).
- [38] P. P. Yang, F. H. Liu, R. Sahoo, *Adv. High Energy Phys.* **2020**, 6742578 (2020).
- [39] P. P. Yang, M. Y. Duan, F. H. Liu, *Eur. Phys. J. A* **57**, 63 (2021).
- [40] CMS Collaboration (V. Khachatryan et al.), *JHEP* **02**, 041 (2010).
- [41] CMS Collaboration (S. Chatrchyan et al.), *Eur. Phys. J. C* **72**, 2164 (2012).
- [42] CMS Collaboration (S. Chatrchyan et al.), *Eur. Phys. J. C* **74**, 2847 (2014).
- [43] CMS Collaboration (A.M. Sirunyan et al.), *Phys. Rev. D* **96**, 112003 (2017).
- [44] ALICE Collaboration (S. Acharya et al.), *Phys. Rev. C* **99**, 024906 (2019).
- [45] ALICE Collaboration (S. Acharya et al.), *Eur. Phys. J. C* **80**, 693 (2020).
- [46] ALICE Collaboration (S. Acharya et al.), *Eur. Phys. J. C* **80**, 167 (2020).
- [47] ALICE Collaboration (S. Acharya et al.), *Phys. Lett. B* **807**, 135501 (2020).
- [48] ALICE Collaboration (J. Adam et al.), *Phys. Lett. B* **760**, 720 (2016).
- [49] ALICE Collaboration (D. Adamova et al.), *Eur. Phys. J. C* **77**, 389 (2017).
- [50] ALICE Collaboration (J. Adam et al.), *Phys. Lett. B* **758**, 389 (2016).
- [51] ALICE Collaboration (J. Adam et al.), *Phys. Rev. C* **93**, 034913 (2016).
- [52] ALICE Collaboration (B. B. Abelev et al.), *Phys. Rev. Lett.* **111**, 222301 (2013).
- [53] ALICE Collaboration (J. Adam et al.), *Phys. Rev. C* **95**, 064606 (2017).
- [54] ALICE Collaboration (B. B. Abelev et al.), *Phys. Lett. B* **728**, 216 (2014).
- [55] M. Gell-Mann, *Phys. Rev. Lett.* **12**, 155 (1964).
- [56] F. H. Liu, *Nucl. Phys. A* **810**, 159 (2008).
- [57] F. H. Liu, Y. Q. Gao, T. Tian, B. C. Li, *Eur. Phys. J. A* **50**, 94 (2014).
- [58] C. Forbes, M. Evans, N. Hastings, B. Peacock, *Statistical Distributions*, Fourth Edition, John Wiley Sons, Inc., Hoboken, NJ, USA, 2011.
- [59] G.-R. Zhou, *Probability Theory and Mathematical Statistics*, High Education Press, Beijing, China, 1984.
- [60] Z. J. Xiao, C. D. Lü, *Introduction to Particle Physics*, Science Press, Beijing, China, March 2016, p. 160.

- [61] Particle Data Group (P. A. Zyla et al.), Prog. Theor. Exp. Phys. **2020**, 083C01 (2020) and update (2021).
- [62] M. Waqas, G. X. Peng, F. H. Liu, J. Phys. G **48**, 075108